2005

Mathematical models for estimating volatile chemical emissions from dredging operations

Kenneth Alexander Fountain
Louisiana State University and Agricultural and Mechanical College

MATHEMATICAL MODELS FOR ESTIMATING VOLATILE CHEMICAL EMISSIONS FROM DREDGING OPERATIONS

A Thesis

Submitted to the Graduate Faculty of the
Louisiana State University and
Agricultural and Mechanical College
in partial fulfillment of the
requirements for the degree of

Master of Science in Chemical Engineering

in

The Department of Chemical Engineering

by
Kenneth Alexander Fountain II
B.S. Mississippi State University, 2000
May 2005

ACKNOWLEDGEMENTS

I would like to express my greatest appreciation to Dr. Louis J. Thibodeaux for the endless guidance, complete support, positive criticism, and efforts to provide unending assistance throughout this research period. I also thank Dr. Kalliat Valsaraj for his help with ideas and discussions throughout the course of this project. My thanks go to Dr. Kalliat Valsaraj and Dr. William Moe for accepting my invitation to serve as committee members for my thesis defense.

I would also like to thank Dr. Ravikrishna for his assistance with the wind tunnel experiment. His previous research proved indispensable to this research. Special thanks are extended to Cindy Price with U.S. Army Corps of Engineers at WES for all the collaboration of data and ideas.

I thank my fellow graduate students for the great discussions in an effort to further the understanding of topics of chemical engineering. Thanks to the LSU Chemical Engineering Department administrative personnel, especially Darla Dao, Danny Fontenot, and Melanie McCandless for all their generous assistance.

I owe all of my success to my parents for their constant motivation throughout my life and their unconditional love. Without their support, none of this would have been possible. Thanks especially to my father for never doubting my potential in life and remaining optimistic.

TABLE OF CONTENTS

LIST OF TABLES

LIST OF FIGURES

LIST OF SYMBOLS

n_A	Mass flux of chemical A, (ng/cm^2-hr)
ρ_{A2}	Chemical concentration in water, (ng/cm^3)
ρ_{A2i}	Chemical concentration in water at air/water interface, (ng/cm^3)
ρ_{A1i}	Chemical concentration in air at air/water interface, (ng/cm^3)
ρ_{A1}	Chemical concentration in air, (ng/cm^3)
ρ^*_{A2}	Equilibrium chemical concentration in air, (ng/cm^3)
ρ^{**}_{A2}	Equilibrium chemical concentration in CDF sediment pore water, (ng/cm^3)
$^1k'_{A2}$	Local water-side mass transfer coefficient at a air/water interface, (cm/hr)
$^2k'_{A1}$	Local air-side mass transfer coefficient at a air/water interface, (cm/hr)
$^1k'_{A2FC}$	Local water-side mass transfer coefficient at a air/water interface in the forced convection zone, (cm/hr)
$^1k'_{A2NC}$	Local water-side mass transfer coefficient at a air/water interface in the natural convection zone, (cm/hr)
$^1k'_{A2D}$	Local water-side mass transfer coefficient at a air/water interface accounting for dredge enhancement, (cm/hr)
$^1K'_{A2}$, $'K_{A2}$	Overall water-side mass transfer coefficient at a air/water interface, (cm/hr)
$^1K'_{A2FC}$	Overall water-side mass transfer coefficient at a air/water interface in the forced convection zone, (cm/hr)
$^1K'_{A2NC}$	Overall water-side mass transfer coefficient at a air/water interface in the natural convection zone, (cm/hr)
H_x	The equilibrium partitioning coefficient for chemical A at a air/solid interface, (dimensionless)

K_{A32}, $^{''}K_{A3}$	The equilibrium partitioning coefficient for chemical A at a solid/water interface, (L/kg)
K_{oc}	The partitioning coefficient of chemical A between octanol and water, (L/kg)
f_{oc}	The fraction of organic carbon within a particle, (dimensionless)
K_{A31}, $^{'}K_{A3}$	The equilibrium partitioning coefficient for chemical A at a solid/air interface, (L/kg)
A_F	Area of DOU with enhanced TSS from dredging activity, (m^2)
A_N	Area of DOU without enhanced TSS from dredging activity, (m^2)
A_{DOU}	The total DOU area, (m^2)
D_{A2}	Diffusivity of chemical A in water, (cm^2/sec)
s	Surface renewal parameter (cycles/hr)
τ_{bucket}	Cycle time of the bucket
n'_{BO}	Oxygen mass flux (ng/cm^2-hr)
E	Specific power delivery efficiency, (dimensionless)
α	Dirty water to clean ratio, (dimensionless)
P	The nameplate horsepower, (hp)
T	The water temperature, (ºC)
ρ_{A2FC}	Chemical concentration in water in the forced convection zone, (ng/cm^3)
ρ_{A2NC}	Chemical concentration in water in the natural convection zone, (ng/cm^3)
ρ_{32FC}	Suspended solid concentration in the forced convection zone, (ng/cm^3)

ρ_{32NC}	Suspended solid concentration in the natural convection zone, (ng/cm^3)
w_a	Chemical loading concentration for bed sediment, (mg/kg)
ρ_{32}	Suspended solid concentration in water, (ng/cm^3)
ρ_b	Bulk density of sediment (gm/cm^3)
n_{ADOUNC}	Chemical flux from the natural convection area of the DOU, (ng/cm^3-hr)
n_{ADOUFC}	Chemical flux from the forced convection area of the DOU, (ng/cm^3-hr)
$\rho`_{A2NC}$	Downstream chemical concentration, (ng/cm^3)
τ	retention time, (1/hr)
h	height of water column, (m)
n_{ADS}	Chemical flux from the downstream area of the DOU (ng/cm^3-hr)
r_o	Radius of the forced convection zone, (m)
ρ^o_{A2}	Chemical concentration in solution in forced convective zone of radial plume dispersion, (ng/cm^3)
D_{A2y}	The horizontal diffusivity of the chemical, (ft^2/s)
r	Radial distance of the plume/embayment from the forced zone, (m)
$\rho_{A2}(r)$	Chemical concentration in water in the natural convective zone at distance r from the forced convective zone, (ng/cm3)
ρ_{A2SS}	Steady state chemical concentration in water in the natural convective zone at outer boundary distance from the forced convective zone, (ng/cm3)
K_o	The modified Bessel function of the second kind, (dimensionless)
P	The delivered mechanical power, (hp)

ε_1	Sediment air filled porosity, (dimensionless)
D_e	the effective diffusivity of chemical A (cm^2/hr)
C_A	The chemical concentrations in air exiting wind tunnel, (ng/m^3)
Q_1	Air volumetric flowrate, (m^3/s)
N_A	The chemical flux to air, (ng/m^2-h)
C_S	Chemical concentration at the surface of the sediment, (mg/kg)
t_b	Time when the water layer is effectively absent from the DM surface (hr)
t_D	Time when the surface is dry of water and pore spaces are primarily air-filled (hr)
t'_d	Surface drying time (hr)
n	Number of patches, (patches)
C_f	Flux calibration factor to exposed DM, (dimensionless)
Q_P	Water flowrate from the dredge site, (ft^3/s)
ρ_{aP2}	Chemical concentration in water in pore water at the DOU site, (ng/cm^3)
Q_B	Flowrate of bulking losses to the CDF sediment, (ft^3/s)
Q_X	Flowrate of pore water from the CDF sediment, (ft^3/s)
Q_S	Flowrate of water to the CDF sediment, (ft^3/s)
Q_R	Flowrate of recycle from the CDF, (ft^3/s)
Q	Total flow of dredged material from the sediment to the barge, (ft^3/s)
ε_2	Water porosity in sediment at the DOU site, (dimensionless)

ε_I	Initial water porosity of sediment/mud at the CDF site, (dimensionless)
ε_F	Water porosity in sediment/mud at the CDF site after consolidation, (dimensionless)
v_s	The velocity of the inlet water flowing into the sediment bed from particle settling process, (m/s)
v_x	The velocity of the CDF pore water flowing into the water column from consolidation process, (m/s)
A_s	The surface area of the CDF, (m^2)
b	An empirical constant, (dimensionless)
C_D	The drag coefficient, (dimensionless)
ρ_2	Density of water at design conditions, (g/cm^3)
l	length of PCDF, (m)
M_a	Molecular weight of the chemical, (gm/mol)
v_1	Wind velocity, (m/s)
$v`_1$	Wind velocity, (mph)
Q_{ds}	DM volumetric flowrate from DOU bottom (ft^3/s)
m_M	Solids in water used to create slurry, (mg/kg)
m_P	Solids in water of stream from dredge site, (mg/kg)
m_R	Solids in water of recycle stream, (mg/kg)
ρ_3	Particle density, (gm/cm^3)
Q	Water volumetric flowrate, (ft^3/s)
ρ_{ao2}	Chemical concentration at x=0 entrance to CDF, (ng/cm^3)
ρ_{32o}	Suspended solid concentration at entrance to CDF, x=0, (ng/cm^3)
A_{stot}	The ponded CDF surface area, (m^2)

ABSTRACT

Dredging operations have been a common remediation for contaminated sediment in an effort to reduce the harmful impact on the environment. The objective of this research was to create models used for estimating chemical release to air from remediating the Indiana Harbor and Canal (IHC) as three separate dredging operations; the Dredge Site, Exposed DM CDF, and Ponded CDF. The evaporative flux estimations are based on a two-resistance mass transport path inclusive of both the molecular diffusion in porous media and interfacial airside mass transport resistances. Several chemodynamic algorithms were used in calculating key transport parameters. Laboratory tests were performed to measure sediment-to-water partitioning and Henry's constant for IHC sediment.

A large portion of the research effort involved investigating by experiments and theoretical models dedicated to the chemical emissions from exposed dredge material. The study of the short term effects of exposure to these contaminants are very important because of the chemical flux quick release at the initial stages from filling and reworking of the dredged material (DM). Data is available for PAH/PCB volatilization from laboratory and pilot-scale flux chamber experiments using DM. However, larger scale or field sites data are required to further validate or test existing predictive mathematical models. A wind tunnel enclosure (16 ft length x 4 ft height x 3 ft width) fitted atop a lysimeter (1.5 ft depth) suited for simulating CDF conditions was used to measure chemical flux release from the DM. Most algorithms previously developed for estimating the chemical release from sediment are based on transport through natural surface soils, which are simpler than those for DM. The latter undergo dramatic physical changes as consequences of water consolidation and evaporation. The model flux estimates were generally lower than the measured ones.

Apparently the copious quantities of water and its upward movement delivered fine particles containing enhanced chemical concentrations onto the surface layer and this higher than bulk concentration was driving the measured flux.

CHAPTER 1

ENVIRONMENTAL DREDGING

1.1 Environmental Remediation

Areas contaminated with hazardous chemicals are potential problems for an entire ecosystem. Pollution is often generated from industrial discharges releasing harmful chemicals into water bodies, which eventually enters the air. With the impact on air quality due to these toxins, risk assessments are performed to determine proper course of action. An evaluation of these changes in the environment can dictate if the impact to the local or global community requires steps to reduce the biological exposure to the contamination. Remediation of contaminated areas involves efforts to reduce the levels of chemical concentration in the water, ground, and air. The most common of these methods for sediment remediation include capping, natural recovery, and dredging; with a combination of dredging and capping in many cases. Other methods of remediation are particle broadcasting, hydraulic modification, and dry excavation (SMWG 2005). Dredging has become the most common practice for large-scale projects in the US due chiefly to the effectiveness of decreasing the chemical concentration by completely or partially removing the bottom-contaminated sediment.

1.1.1 In-situ Capping

Recent research interests are moving towards applications of sediment remediation using a capping system. Generally, a capping system entails covering underwater sediment locations containing high chemical concentrations known as “hot spots” with solid materials. The cap consists of a stable cover using layers of clean sediment, gravel, stones, and/or synthetic materials for reducing chemical mobility and blocking organisms from bioturbating

the contaminated sediment (NFESC 2005). The caps typically range from 30 cm and 100 cm in depth. The capping material prevents the chemical in pore water from entering into the water column above it. Although some materials are best suitable for reducing or eliminating this chemical diffusion, installation of the cap and resilience to harsh conditions can often produce significant limitations to the effectiveness of a capping system. Current research deals with establishing caps designed to chemically react with the hazardous chemicals in order to reduce or eliminate the potential biological impact. A major roadblock for this technology deals with the scale-up and implementation from laboratory to the large-scale environment.

1.1.2 Natural Recovery

There are some situations that permit doing nothing as the most practical solution to a remediation project. This results from nature having the ability to remediate itself. Although an uncommon approach, natural recovery may produce a natural reduction of chemical concentration in the sediment over time. The chemical will eventually disperse to the point of being non-hazardous due to the environments pursuit for restoring equilibrium. This is generally a case for a site with low initial levels of chemical concentration. The cost of the other remediation methods and the nuisance of long periods of the mechanical activities can make natural recovery a better choice. This practice is less common in most remediation projects due to the long period of time for the reduction to occur. In the case of sites with large amounts of pollutant, a more active effort must be made to prevent long-term exposure to the surrounding ecosystem.

1.1.3 Environmental Dredging

Dredging was originally developed for navigational uses important to large vessels traveling on waterways. As nature is constantly changing, so are the navigated waterways. Bottoms of rivers, canals, and harbors accumulate with sediment and debris over time from storms and natural disasters. Often, it is necessary to remove the sediment to provide a safe depth for motor vessels. The dredging may also be performed to change existing channel pathways and provide others in efforts of optimizing transportation period of raw materials. The Army Corps dredges about 250 million cubic yards of maintenance material from the US waterways annually (Global Security 2005).

Its uses have been making an increasingly profound impact on environmental remediation efforts in the US. This process of removing the contaminated sediment from the bottom of the water column can provide significant reductions in the sediment chemical concentration. The two primary techniques for the removal process involve transporting the sediment from the water either mechanically or hydraulically. The dredges operate by using an arm with a bucket attachment used to excavate a volume of sediment at the bottom and return to the surface. As the importance of reducing the resuspension became essential to mechanical dredging, advances to the buckets designed provided significant contributions to mechanical dredging. Technical modifications to the attachment were made to remove a section of sediment with effort to minimize the disturbance to neighboring sediment and reduce the resuspension of solids. After the sediment is collected, it is transported to the surface by means of the mechanical arm or the suction process of the hydraulic dredge. The sediment is then transported to a nearby confined disposal facility (CDF) using either transport trucks or hydraulic pipeline. The sediment will either consist of ~ 50% solids

forming exposed mud patches with the former or ~5% solids forming a ponded CDF with solids depositing to the bottom with the latter. When piped into the CDF, a treatment center is commonly used to remediate the water leaving. Mechanical dredging can utilize both transportation methods, whereas hydraulic dredging requires a pipeline to the CDF. Two situations occur once the sediment enters into the CDF. After filling close to the top with solids, the CDF is capped most often using sand. This process can require a project period from 10-30 years.

The design of the dredging process requires the knowledge of cost, location, and biological impact. These factors will designate particular alternatives of dredging in effort to find a practical method to reduce the chemical exposure to the environment. With some exceptions, dredging entails several steps and parts. A site of concentrated contaminated sediment is defined commonly with a silt curtain as the Dredge Operable Unit (DOU). A barge containing the dredge component is positioned on the upstream side of the DOU. As dredging commences, the dredge arm reaches to the bottom of the DOU and transports the sediment to some transport device. The sediment is then transported by either motor vehicle or hydraulic pipeline to the desired disposal site. The disposal site is a predetermined site to reduce both exposure to the environment and cost.

1.2 Dredging Equipment

The mechanics of dredging have been well developed for the purpose of transferring contaminated sediment from a polluted water site to a disposal site. Since the original focus of dredging dealt with moving sediment for navigational purposes, modifications were required on the machinery to ensure more efficient capture of in-situ material. Advances to the dredging technology include improving the dredge accuracy, decreasing suspended solid

generation, reducing spill layer, and replacing automation for manual controls (IADC 2005). As shown in Figure 1, the selection of devices for the remediation projects includes in either mechanical or hydraulic dredging. Since the 19th century, dredge mechanics have changed dramatically due to the further developments of steel, computers, and satellite navigation. Dredges are now much larger and stronger with a high level of automated control, removing the manual "feel" control of the operator.

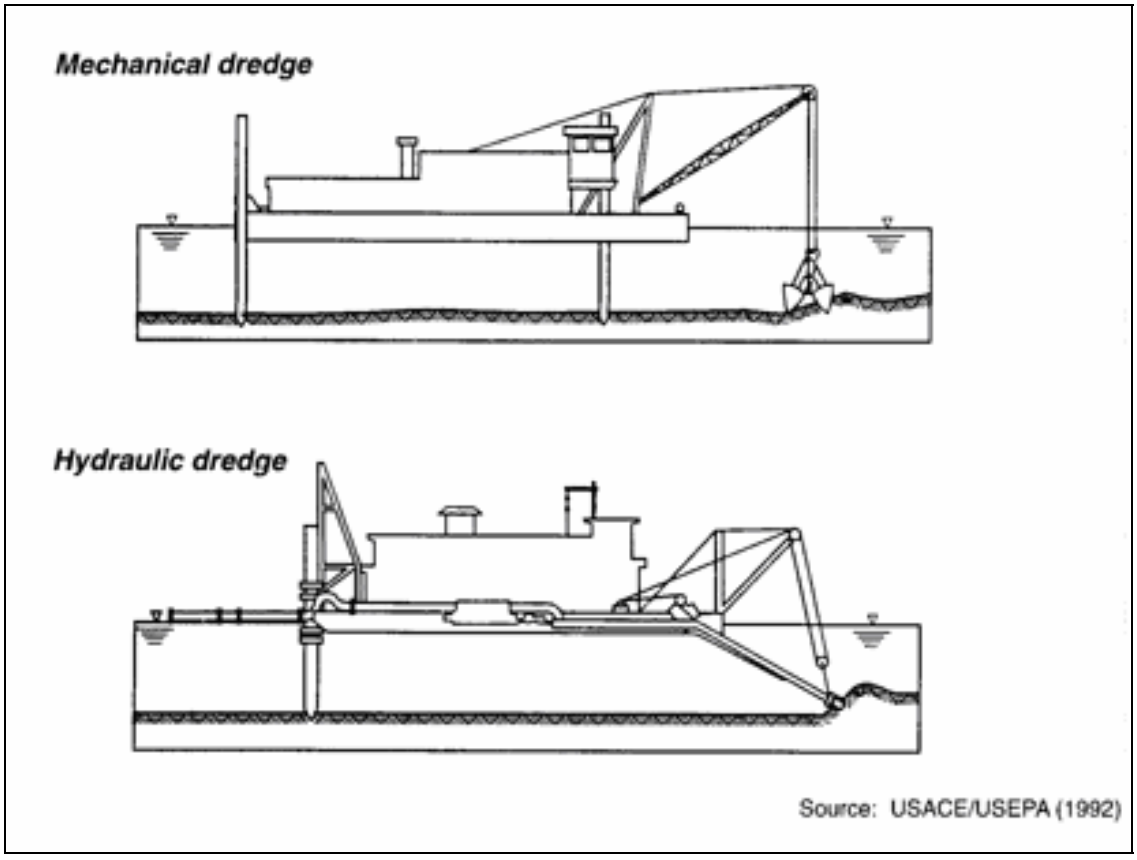

Figure 1.1 Mechanical and Hydraulic Dredges

1.2.1 Mechanical Dredge

One of the most commonly used dredges in remediation is the mechanical dredge because of its versatility. The option of reaching larger depths and operating under undesired weather/flow conditions make the mechanical dredge often more suitable than the other

dredge devices. The mechanical or bucket dredge consists of a bucket or scoop located at the end of an extending arm connecting to the barge. Most common of the mechanical dredges are those with either a dipper or clamshell tip. These dredge heads can accommodate dredge volumes commonly of the range of 2 to 10 m^3 each dredge cycle (ARCS 1994). This excavation process can remove material close to in-situ. Sediment losses from the dredging process occur mostly at the bottom of the water column. However, significant amounts of losses can also occur from the mud coated bucket moving through the water column and exiting the water depending on the design of the dredge head. The consistency of the dredge material (DM) upon being deposited on the barge is normally around 50% solids with the balance mostly water. Operational controls include smooth hoisting of the bucket and use of a hoisting speed less than 2 m/s (ARCS 1994). The sediment is transported by one of two ways: motor vehicle devices or hydraulic pipeline. In the case that the sediment is transported hydraulically to the disposal site, sediment slurry of ~5% solids is created either at the barge or on the shore.

1.2.2 Hydraulic Dredge

In order to reduce total suspended solids (TSS) in the water column, hydraulic dredges prove to be the most appropriate when excavating sediment under low flows and limited depths. This device is designed using a pump on the barge to create a vacuum pipe suction head. Usually the sediment layer must be broken up into smaller refined particles able to be transported up to the barge. Cutting blades in the suction head are used to crush and lift the dense and rocky sediment bottom. These blades are either aligned horizontally (auger dredge) or vertically for rotation prior to the suction opening. These dredge heads typically range from 0.3 to 1.0 m in across the blade opening with a swing arm up to 30 m

across and swing velocity of 0.5 m/s. These dredges can often generate significant particle resuspension at the benthic layer, but at TSS of lower concentration since these particles remain at the bottom of the water column and redeposit to the surface. The hydraulic dredge requires the sediment to be transported from the barge to the disposal site hydraulically due to the enormous volume of water transported along with the contaminated solids. The hydraulic dredges are generally used in low water flow conditions due to barge platform stability problems. Horizontal dredges are used to collect 50 to 120 yd^3/hr and are useful for small projects where solid resuspension is a major concern (ARCS 1994). Typical volume flowrates of sediment dredged using hydraulic dredges are around 1 to 10 m^3/s.

1.3 Dredge Material Disposal

Sediment removal involves two parts, excavation and disposal. After being removed from the bottom of the DOU, the sediment is moved from the dredge barge to the disposal site by two methods. If mechanically dredging, motor vehicles (i.e., trucks, hoppers) can be used to continuously move the DM to the disposal site. The standard dump truck can transport ~ 3.8 m^3 of dredge material each run, requiring several hundred thousand loads made for a large scale project (GLDT). Therefore, this method of transport can pose significant cost issues as well as time and resources. In most cases, the tops to these trucks are open which involves the issue of chemical emissions during transport to the disposal facility. The use of hydraulic pipeline transport of the DM minimizes these drawbacks of motor vehicle transport. The DM requires a decrease in density by the addition of water in creating slurry. By adding water to the DM, another concern develops as to the inevitable requirement to treat the added water. The focus for cost will diverge to the comparison of the fuel and resource for vehicle transport to the treatment of the added water. Hydraulic

dredges will require hydraulic pumping, thus, eliminating this comparison and focus attention to the reduction of the amount of water leaving the disposal facility by way of minimum water added and/or adding a recycle loop.

There are two options of sediment disposal, open water and inland; both common and dependant on the site. The method of discarding DM to open-water has been used when the site is located close to the sea. Biological impact may be significant, for these and other reasons the open water disposal method is not always applicable or feasible. When the dredge site is closer inland, a large landfill called a confined disposal facility (CDF) can be used to store the dredge material transported from the DOU. There are two types of CDFs that are designed for disposing DM; near shore or upland. The design configuration of the CDF can vary from one or more basins. The size and design of each CDF is site-specific, depending on the location, the nature and potential amount of sediments and how it will be used or function once it is full and/or no longer receiving dredged material. The CDF is commonly filled at one specific side of the CDF producing a slope in sediment on the floor. In the case of mechanical transport, the sediment is spread over the bottom maintaining a gradient in height to collect water in a small area where it will be pumped out of the CDF. The other scenario deals with the CDF being hydraulically filled and creating a pond that also contains a sediment sloping bottom due to the larger particles depositing at the entrance. CDFs are typically constructed with a liner such as clay to prevent seepage into the ground water. It is also capped with a material such as clay after being filled with sediment and allowed to dry.

1.4 Indiana Harbor and Canal

The model discussed in this report was developed for use in evaluating chemical emissions from the Indiana Harbor and Canal (IHC). It is located in East Chicago, Lake County, Indiana. There are ongoing plans for US Army Corps of Engineers (USACE) to dredge the sediment as an aid to navigation. Figure 1.2 shows the proposed layout of the CDF cells. This site was determined to require remediation in specific areas due to the high levels of contaminants such as PAHs, PCBs, oil & grease, chromium, and lead. The Chicago District of the USACE is developing plans for the method of remediation based in part on the analysis and results of volatile emission predictions using the following models.

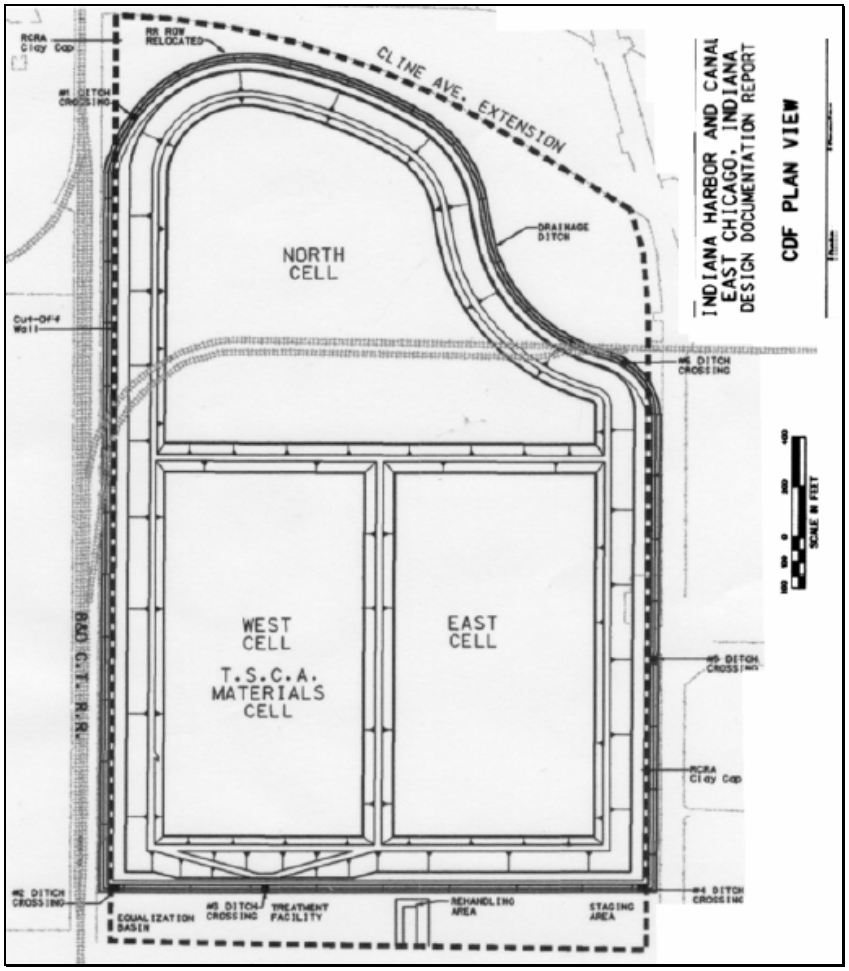

Figure 1.2 IHC CDF Design Layout

Table 1.1 IHC Sediment Analysis

Compound	Concentration, ug/kg
Naphthalene	2650
Phenanthrene	6930
2-Methylnaphthalene	1760
PCB-1248	5103
PCB-1260	500
Chromium	290
Copper	213
Lead	437
Zinc	2440
Manganese	1560
Total Organic Carbon	96000
Oil & Grease	3.29x10^7

CHAPTER 2

GENERAL MODEL THEORY AND BACKGROUND

2.1 General Model Development

In evaluating the fate of chemicals in the environment, fundamental concepts are presented to describe the behavior these interactions. The mobility of a species is defined using a mass balance around a system of chemical gradients. These quantity variations form the basis for the chemicals ability to transport themselves through medians and across interfacial boundaries by various mechanisms. The transfer involves the movement of chemical in the environment between the atmosphere, hydrosphere, and geosphere. The geosphere represents the primary focus of these models since they include both water bodies and soil-like surfaces

2.1.1 Soil Models

A literature review of chemical volatilization from sediment or dredge material was performed to determine current theory and transport models available for application to dredging. Most of the applications for this theory are designed for use in the modeling of volatilization of chemicals from dry soil. Early work on chemical volatilization surrounds the emissions of pesticides to the atmosphere from dry soil on farmlands. This research began to unfold as scientist discovered that in the absence of appreciable mass transfer due to water movement, diffusion processes in the soil account for the movement of pesticides to the soil surface to replace that lost by volatilization (Mayer et al. 1974). The research analyzed several models against volatilization data to find that indeed under negligible wind speeds, the surface was still renewed through diffusion in the pore space. This matched closely to the experimental values compared to the models assuming that the concentration

goes to zero under these conditions. This showed the process to be diffusion controlled instead of through interfacial resistance. Most of the models of this time were directed towards specific conditions instead of general transport processes. Further work was performed by scientist from University of California Riverside and USDA showing the critical process of gas phase molecular diffusion on the process of surface concentration renewal. The research was intended to supply a general volatilization model for estimating pesticide emissions from soil (Jury et al. 1980; Jury et al. 1983; Jury et al. 1984(a); Jury et al. 1984(b); Jury et al. 1984(c)). A more complex model by Cohen et al. (1988) showed that the volatilization model could assume a linear isothermal diffusion neglecting natural convection within the soil to adequately describe the chemical flux at long times.

The soil models previously developed are not representative of modeling volatilization from DM because of the difference in pore space composition and compaction. For natural soil models, the pore spaces typically contain some air. In these models, the soils are completely consolidated. In consolidated soils, the solids have compacted themselves thru gravity settling processes to the point of a negligible to no change in pore space volume. The exposed DM process is dynamically changing with time with pore spaces changing from completely water-filled to air-filled through evaporation and consolidation occurring throughout this process. This ongoing consolidation process acts to provide a driving force for water movement in a CDF. Downward movement is retarded due to the floor being nonporous.

A recent literature review by (Thibodeaux et al. 2002) comprised a model to simulate volatilization from dredge material and soils. The purpose of this model was to define the process of volatilization by using a simple equation based on a Lavoisier mass balance

around the soil column assuming semi-infinite boundary conditions. The equation provides estimates based on describing the chemical pathway of desorption from solid particles into the water film, desorption from being in pore water solution to pore air, gas phase molecular diffusion to the surface, depletion of surface concentration over time, resistance of solid/air interface transporting to the bulk air above.

Modeling drying dredge material is required for estimating emissions from dredging operations since it transpires regardless of the method of transporting the sediment to the CDF. When the sediment is truck-delivered to the CDF post mechanically dredging, the material arrives at the CDF as drying mud. In the event of hydraulically transporting the DM to the CDF, the water layer above will eventually be removed producing exposed drying mud. In all cases of dredging, the emissions from the drying DM will be of high importance due to the direct contact for the chemical in mud with air. This drying mud process may provide significant emissions to air with an impact on the local environment.

2.1.2 Water Models

The following models deal with the chemical interactions between liquids and gases. The case of emissions from a DOU or Ponded CDF requires mass balances are conducted to provide aqueous chemical concentrations in the water column for estimations of the chemical evaporation to the air. For both of these processes, the balance is performed under steady state conditions. In representing these phenomena, the concepts of developing theory surround both a driving force and its resistance. Chemicals placed into one of these mediums will transfer a portion of the initial concentration into the adjoining phase for equalization. Each phase will contain a chemical flux shown in Equation 1 that are equal and opposite operating as the flux of chemical from water to air.

$$n_A = {}^1k'_{A2} \cdot (\rho_{A2} - \rho_{A2i}) = {}^2k'_{A1} \cdot (\rho_{A1i} - \rho_{A1}) \quad (2.1)$$

The chemical transport from water to air is dependant on the resistance to mass transfer across the interface and an overall chemical concentration gradient, $\Delta\rho_{A2}$. It is the concentration gradient that acts as the driving force for the movement of chemical from the water to the air. For a given chemical concentration in air, there is an associated equilibrium concentration in the water, ρ^*_{A2}. Mass transferred across the air-water interface occurs when the equilibrium concentration within the air is less than the water concentration. The overall evaporative flux of chemical A across the interface is:

$$n_A = {}^1K'_{A2} \cdot (\rho_{A2} - \rho_{A2}^*) \quad (2.2)$$

While the concentration gradient drives the system to equilibrium, the mass transfer resistance controls the rate of transfer. The overall mass transfer coefficient of chemical from water to air, ${}^1K'_{A2}$, is comprised of local mass transfer coefficients (MTC) on both sides of the interface as dictated by the two-resistance theory. The chemical emissions to the air are defined using the fundamental component material balances.

The resistance to mass transfer is given by the two-resistant theory equation:

$$1/\,{}^1K'_{A2} = 1/\,({}^2k'_{A1} \cdot H_x) + 1/\,{}^1k'_{A2} \quad (2.3)$$

where: H_x- dimensionless Henry's constant

Both the airside and waterside mass transfer coefficients will determine the rate to which chemical emissions cross through the interface into the bulk air phase. This theory has been well established in defining chemical transport resistance between two adjoining phases with interfacial equilibrium.

2.1.3 Phase Equilibrium Process

The process critical to correctly modeling chemical volatilization is the sorption potential for a chemical to distribute between two phases. This capacity will determine the degree to which a chemical will be released through the pathways for emissions. In the DOU and CDF, the Local Equilibrium Assumption is assumed to between water and solids in the pore spaces and suspended solids in the water column. A true equilibrium is never established, so pseudo-equilibrium is assumed to characterize the distribution of chemical between the aqueous phase and solid particle. A local equilibrium subsists in the pore spaces of dredge material when the rate of water movement past the solids is at a slow enough velocity. This Local Equilibrium Assumption (LEA) can be made to provide reasonable estimations for chemical concentrations (Schroeder, P. R. 2000).

It has been established that chemicals in phase equilibrium with solid particles are dependant on the fraction of particle organic matter. The partitioning between solid-water, K_{A32}, is linearly dependant with the soil organic carbon-water partitioning, K_{oc} by the following expression:

$$K_{A32} = f_{oc} \cdot K_{oc} \tag{2.4}$$

where: f_{oc} = fraction organic carbon

This partition coefficient is used in all of the following models for determination of the water equilibrium concentration in pore space and in the water column from suspended solids.

Also very important to modeling these processes are the equilibrium estimations for solid-air, K_{A31}, and the Henry's constant for air-water, H_x. The estimation of K_{A31} for wet sediments/soils can be determined using the following relationship:

$$K_{A31} = K_{A32} / H_x \tag{2.5}$$

The expression above is used in the estimation of equilibrium concentrations in the sediment modeling emissions from exposed DM. It establishes the driving force concentration gradient along with the background air concentration required in the flux equation. The sorption processes among solids and air/water have established much discussion over recent years as to the exact nature of equilibrium. Most ongoing research has been focused on the providing better descriptions of the equilibrium interactions between chemicals in air or water and the specific type of organic matter of a solid.

2.2 Dredging Models

The chemical emissions from dredging operations are compromised of three sources. These include the dredging operable unit (DOU), the DM transport devices, and the final disposal site. All may generate significant emissions to the air to possibly affect the local and remote environments. In this research, focus was directed towards the estimations from the DOU and CDF. The transport device model was outside the scope due to the basis of using hydraulic pipeline transport to the CDF. For mechanical dredging, transporting the DM to the CDF can be performed hydraulically by creating slurry. Emissions can occur at the input to the CDF. The slurry source is lumped into the DOU model while the discharge is modeled in the CDF model. Because of the mode of operation, the CDF may contain two types of scenarios exposed dredge material and ponded that require the development of two separate models. The following discussion will highlight the development of three models developed to estimate chemical evaporation from these sources to quantify chemical exposure in the neighboring ecosystem.

2.2.1 DOU Sources

In the case of dredging, the water from the DOU area and the barge (in the case of mechanical dredging) will contain solid to water desorption processes. In the case of chemicals with low partition coefficients, the water will become very concentrated with chemical allowing high chemical fluxes to the air above. The important factor in this process is the involvement of suspended solids. For the case without dredge activity, chemical concentration in the water column is generally controlled by the diffusion of chemical from the sediment pore water at the benthic layer. As dredging commences, the turbulence within the DOU produce a well mixed body of water consisting of a high concentration of suspended solids. These suspended solids will act as a generation term of increasing the water column chemical concentration.

Developments with the DOU model distinguish source areas with and without enclosures. It further depicts dredging enclosures for a flowing river and for embayments. The different scenarios for the DOU models result in a total of three cases for emissions in the DOU area. All of these cases involve the mass transfer resistance distinction between forced and natural convection due to an increased turbidity at the dredge. The downstream conditions will be dependant on the use of silt curtains inhibiting both flow of water and solids outside the DOU. These different design conditions require the model to accommodate situations with and without enclosures in flowing water bodies along with embayment waters. The DOU model is based on theoretical descriptions defining steady state transport processes form dredging.

2.2.2 CDF Sources

2.2.2.1 Hydraulic Transfer to CDF

When hydraulically piping DM slurry into a CDF, a pond of water is formed with solid particles depositing based on diameter from largest to smallest from the entrance to discharge. This inflow of slurry material is modeled with a constant inlet location at steady state conditions. At steady state, the CDF contains a flux in of chemical from the sediment bottom along with a flux out from evaporation of chemical to the air. A mass balance is performed over the system to estimate the concentration in the water column over the length of the CDF. This concentration will change as a function of distance from the inlet and accommodations are made for this, but a particle mass balance is not performed. A unidirectional approach in the x-direction is used in a plug-flow model instead of mixed tank model to estimate worst-case concentrations.

The ponded CDF operation period ends when the water is removed to allow drying of the DM. Improper drying of the sediment can lead to weak bed structure within the area and difficulty in providing a final cap. The CDF normally drains opposite the inflow nearby the treatment facility. As this draining occurs, sections of the CDF become exposed to air. This transient process begins to emit surface chemical from the pore space as it slowly changes from completely water-filled to air-filled from evaporation. The evaporation process is very important since diffusion through air is far greater than water. This process will show to be extremely significant in estimating the release of chemical in a CDF.

2.2.2.2 Mechanical Transport to CDF

If mechanical transport of the sediment is performed, the process of ponding the CDF will not occur. Thus, the CDF will begin with emissions directly from exposed dredge

material instead of going from ponded to exposed DM. The modeling of this case will begin with the evaporation of water in the pore space.

CHAPTER 3

DOU EMISSIONS MODEL

3.1 Model Development

3.1.1 DOU

The chemical release from the dredging site is a function of factors such as dredge operation and process design conditions. The operation begins with a design plan to determine the actual area of dredging. This section of the water body is known as the dredge operable unit (DOU). Most remediation actions occur in two primary locations: rivers and embayments. This classification of DOU designs makeup three different scenarios as shown in the Figure 3.1.

A common case of dredging involves enclosing a section of a flowing river as shown in Figure 3.1a with a silt curtain. This curtain inhibits suspended solids from exiting the DOU. Depending on the efficiency of the curtain, the water downstream of the DOU will produce chemical evaporation to air primarily due to chemical remaining in solution from the exiting DOU water flow. The DOU area will contain higher concentrations due to the large area of suspended solids due to dredging.

The DOU in Figure 3.1b is similar to the previous DOU except for the fact that it does not contain an enclosure around the DOU area. The absence of the enclosure results in a DOU modified area because of suspended solids moving directly downstream of the forced zone surrounding the dredge. Previously, suspended solids were contained within a non-flowing zone. This case is very similar to modeling a ponded CDF in that the forced zone will act as the input to the CDF with an exponential decay of suspended solids downstream.

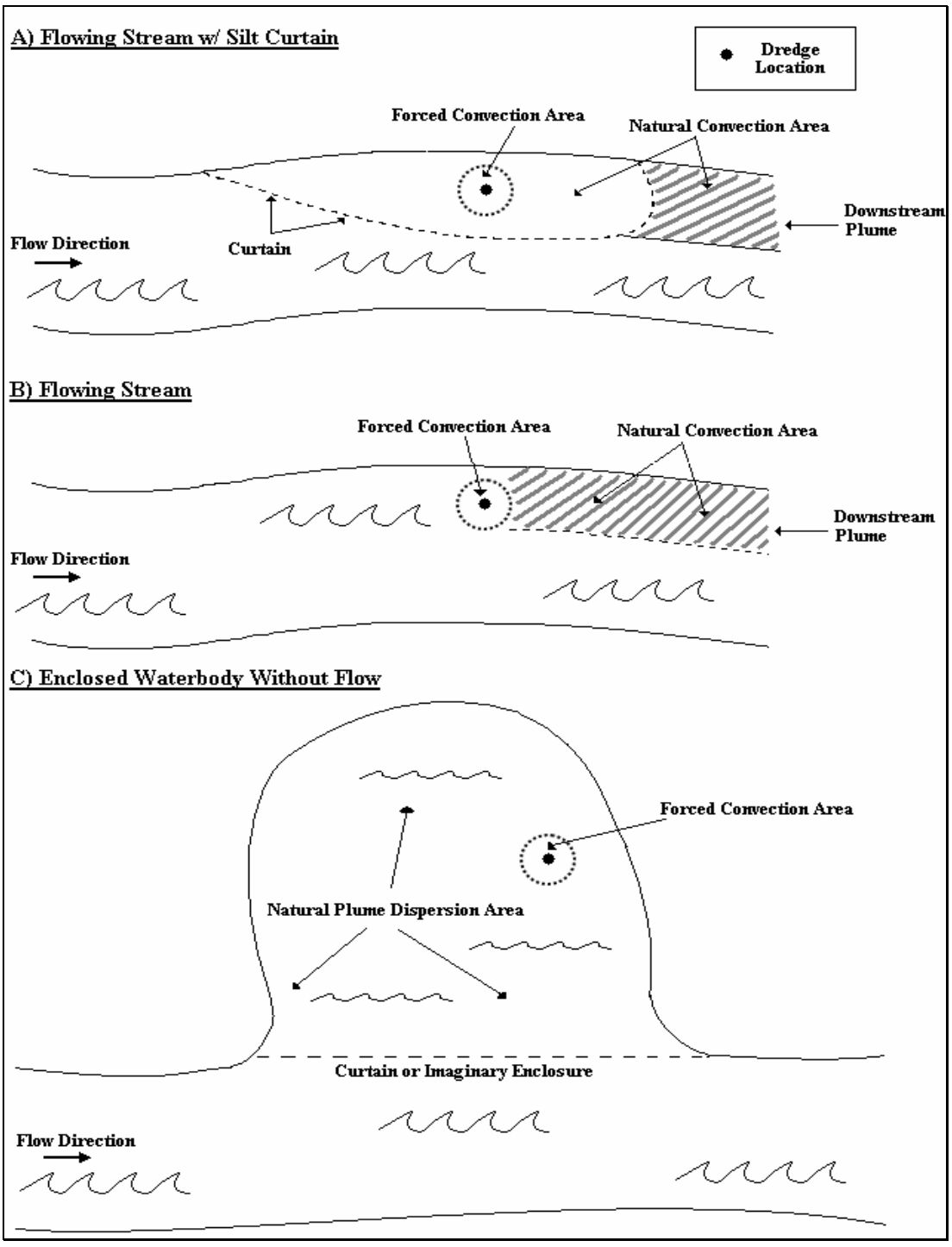

Figure 3.1 Forced and Natural Zones of DOU

The scenario depicted in Figure 3.1c, dredging is performed inside a harbor or bay. There is hydraulic flow inside the enclosure. This case is handled differently from the

previous DOU types because of the no flow condition. This will establish a dispersion effect on the chemical surrounding the dredge. The dispersion of chemical from a point source occurs from chemical diffusion through water in the radial direction. The chemical diffuses through water primarily due to concentration gradients, which exist from the source to the edges of the embayment. The model will compensate for the chemical dispersion from the dredge without advection.

3.1.2 DOU Mass Transfer Coefficients

Both natural and forced convection processes can occur on either side of the interface and the magnitude of the coefficient is controlled by the degree of turbulence. Under static conditions, no flow of water and wind, the chemical movement will depend on the slow rate of diffusion through the water and air. With wind and water movement, the turbulence in both these phases increases, the turbulent eddies propels the chemical in the water to the interface and away from the interface in the bulk-air. So the level of fluid convective turbulence heavily influences both the local waterside and airside mass transfer coefficient.

The characterization of turbulent driven processes has been a highly researched area in chemodynamics over recent years and numerous correlations exist. The natural convection-induced mass transfer coefficients are fairly well understood and correlations exist. Thus, the natural convection mass transfer coefficient can be determined using appropriate equations mentioned in following sections. Those used to determine the forced convection induced mass transfer coefficient will require further evaluation since mechanical turbulence generation is very "device" specific. It is becoming increasingly important to develop better coefficients for estimating chemical emissions. There are currently no empirical expressions developed specifically for estimating dredge induced mass transfer

coefficients. No studies have been performed for dredge operations so that approximate alternatives are reviewed below that may provide reasonable estimates. These methods, based on existing theories and similar mechanical devices, are expected to give only reasonable approximate values.

As currently being used, it is convenient when estimating emissions to air to create so called "forced" or "natural" convection mass transfer coefficients area zones; see Figure 3.2 (Springer et al. 1984). By the separation of these two processes into different area zones, the estimation for emissions produces a more accurate account of the transport processes under the influence of mechanical disturbance (i.e., forced and natural). In accounting for the different fluxes for each zone, Equation 1 becomes:

$$n_A = (({}^1K'_{A2FC} \cdot A_F + {}^1K'_{A2NC} \cdot A_N) / A_{DOU}) \cdot (\rho_{A2} - \rho_{A2}^*) \quad (3.1)$$

where: A_F = area of DOU with enhanced TSS from dredging activity

A_N = area of DOU without enhanced TSS from dredging activity

A_{DOU} = the total DOU area

Figure 3.1 also illustrates these zones within each of the DOU scenarios containing for the respective areas. Combining both the area in the DOU with forced convection and natural convection will give A_{DOU}. In Figure 3.2, the circular zone shown surrounding the dredge contain wind hydraulic and mechanical turbulence is referred to as the forced zone, A_F, while the area beyond is influenced by wind and hydraulic turbulence only is designated as the natural zone, A_N. The means for estimating these two areas is given later in the report.

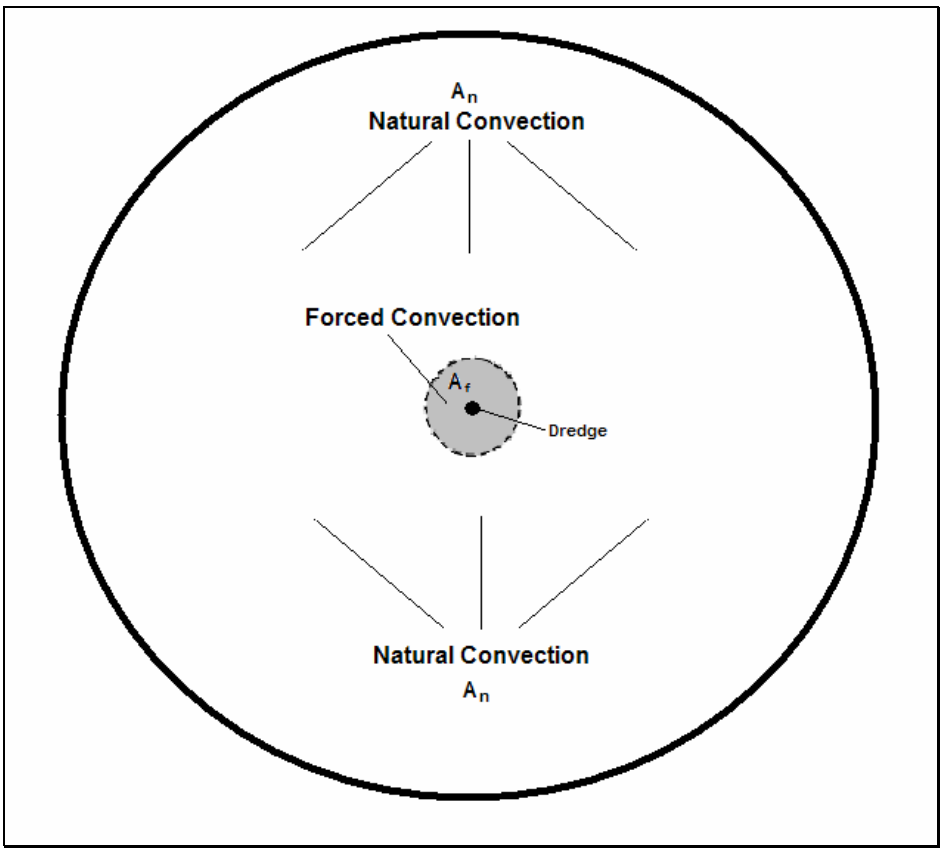

Figure 3.2 DOU Convection Zones

3.1.2.1 Forced Convection Zone

3.1.2.1.1 Liquid-Side MTC

In a forced convection process, a mechanical device primarily generates the fluid bulk flow turbulence. Since the transport of chemical in the bulk fluid phase can also be attributed to natural forces, the combination of waterside mass transfer coefficients in the forced zone becomes:

$$ {}^{1}k'_{A2FC} = {}^{1}k'_{A2NC} + {}^{1}k'_{A2D} \qquad (3.2) $$

The mechanical effect used to characterize the increase of turbulence in the water column may be estimated from equipment such as mechanical/hydraulic dredges, aerators, and boats.

In a following section, details on this forced convection liquid-side mass transfer coefficient induced by mechanical and hydraulic dredging will be developed.

3.1.2.1.2 Air-Side MTC

This aspect of mass transfer has been well-established and appropriate equations area available to estimate ${}^{2}k'_{1A}$, the airside mass transfer coefficient. The mechanical devices analyzed in the following discussion are assumed to create significant disturbance to the liquid-side mass transfer and not to the airside. Chemical transport from the interface to the bulk airflow will occur through natural convection only by way of wind. Details will be developed following a discussion of dredges.

3.1.2.2 Dredge Characterization

An effort is placed towards closely representing the operational aspects of both mechanical and hydraulic dredges and its influence on water turbulence. The mechanical dredge bucket moves up and down through the entire water column to physically act upon the entire vertical distance from bed to surface of water column to define the forced convection zone. Although not moving vertically, the cutterhead/auger of the hydraulic dredge can produce turbulent eddies throughout the water column with the suction activity and side-to-side sweeping motion of the ladder at the bottom of the water column. The near bottom turbulence is likely greater. The cutterhead/auger suction section moves water along with sediment from the bottom, inducing water currents up to a certain height in the water column that because of continuity must also have a downward direct component. To a lesser degree, the hydraulic dredge arm (i.e., ladder) connecting the cutterhead/auger to the dredge barge stirs the entire water column; more so near the bottom than the surface. This displacement of water causes yet unexposed water containing chemical to be transferred

upward towards the surface, elevating the concentration at the interface to provide the increase in emissions to air of the chemical in solution.

In the development of the mass transfer coefficient for mechanical and hydraulic dredges, the understanding of the increase turbulent eddies creating additional movement and displacement of water at the surface enables estimations using similar representations of this process. Such processes will be discussed in following sections with the fundamental idea to represent the increased rate of water transport and turbulence to and from the interface. These processes enact both the ideas from a theoretical or fundamental perspective. Each of these processes is characterized for mechanical bucket dredging only, hydraulic dredging only, or for both.

3.1.2.3 Surface Renewal Model

The theory of surface renewal was first developed by Dankwerts in 1951 to describe the resistance at the air-water interface for a general mass transfer process. Originally, the penetration theory was developed for surface water existing up to some age and then cycling through turbulence to replace the surface waters. In developing the surface renewal theory, Dankwerts purposed the correlation of the rate of renewal parameter, s, to describe the age of exposure. He chose an exponential distribution function for s with the adjoining phase renewal rate for a realistic approach to the process. By the determination of s, a measure of fluid turbulence induced by mechanical devices could be made to determine the resistance to mass transfer across a phase boundary. As the renewal rate increases, the fluid will begin to change from being solely controlled by diffusion through a fluid. The transport processes will then include a convection and diffusion operation resulting in the chemical emissions increasing. Using the exponential function to describe the distribution of surface water ages,

the mass transfer coefficient, ${}^{1}k'_{A2}$, of chemical A is related to the diffusivity of chemical A in water, $\mathcal{D}_{A2}$, and, surface renewal parameter, s, by:

$$ {}^{1}k'_{A2} = (\mathcal{D}_{A2} \cdot s)^{1/2} \qquad (3.3) $$

where surface renewal rate, s, contains the units, sec $^{-1}$, and the diffusivity coefficient in water, $\mathcal{D}_{A2}$, with cm^2/sec. If the diffusivity of the chemical A in water is assumed constant, the mass transfer coefficient will vary directly with the square root function.

The renewal rate describes the increase chemical emissions when mechanical dredging as a constant representing the idea of an exchange of surface water in periods. The mechanical dredge can be represented using this theory because of the bucket motion up and down through the interface roughly mimics the renewal rate concept. The s should be closely related and proportional to the cycle time upward and downward of the bucket through the water column. As the bucket passes through the interface either up or down, the turbulence will dissipate much like the waves from a pebble thrown into water. In representing s as the cycle time of the bucket (τ_{bucket}), the relationship between the two variables is as follows:

$$ s = k / \tau_{bucket} \qquad (3.4) $$

where k is some proportionality constant. Adding the cycle time the bucket travels both downward and upward through the water column can be used in estimating τ_{bucket}. The variable k is unknown in this basic approach; alternative approaches must be considered.

3.1.2.4 Surface Aerator Model

Representing the dredge as a surface aerator makes a more convenient and practical characterization of determining the mass transfer coefficient for forced convection of the dredge. The surface aerator generated MTC was studied vigorously in the mid 1900's in order to increase the oxygen concentration in the water. Over the past few decades, the

concepts have been optimized and are now well understood. A surface aerator is designed to sit at the surface of a water body with about half of the device under water. The mid section contains a set of rotating paddles or blades that stir the surface of the water column. This action produces a great deal of reaeration to the water column by providing a larger amount of bulk water exposure to the interface. The process of air strippers involves displacing the surface water laterally from the center of the aerator so that bulk water from below will rise up and emit the chemical in solution. A turbulent water column is then developed while the surface water will move out to the sides to get moved down by continuity to replace the bulk water moving up to the surface. It essentially is the practical idea for surface renewal and roughly mimics the up and down movement of the dredge bucket. Both operations constantly displace the chemical diluted surface water that has emitted some quantity of chemical to the air with chemical concentrated bulk water. This water turnover device produces a continuous cycle of renewal.

Although the ideas of how the surface aerator increases emissions to the air, the developing equations for estimating the forced convection mass transfer coefficient can entail more complexity. The primary reason for being able to represent a bucket dredge with the surface aerator is that the development of the aerator was done so by using the power of the mechanical device as the primary and essential variable in the equations. The plan is to develop a correlation between these equations using aerator power input to that for the dredge. Conceptually, the bucket dredge will not produce quite the disturbance found from an aerator. Instead of remaining at the surface to vigorously renew the surface, the bucket dredge moves up and down the water column producing high energy turbulent eddies that causes a trailing water flow behind the dredge while side bulk water moves to the surface for

replacement. Once the bucket dredge moves past the interface, the renewing of the surface with chemical concentrated water will decrease exponentially until the dredge reaches some depth where the water does not impact the surface.

For estimating the mechanical dredge contributions to the overall waterside mass transfer coefficient, correlations were defined using the concepts mentioned above. The following equation modified and generalized from the original oxygen form is (Thibodeaux 1996):

$$^{1}k'_{A2} = 3140 \cdot (\mathcal{D}_{A2} / \mathcal{D}_{B2})^{1/2} \cdot (n'_{BO} \cdot E \cdot \alpha) \cdot (A_F/A_{DOU}) \cdot (1.024)^{(T-24^{o}C)} \qquad (3.5)$$

where B- oxygen; n'_{BO}- the oxygen delivery, 2 to 4 lb O_2/hr · hp; E- specific power delivery efficiency of 0.65 to 0.9, dimensionless; α– dirty water to clean ratio, 0.8 to 0.85, dimensionless; P- the nameplate horsepower, hp; T- the water temperature, ºC.

3.1.2.5 Motor Vessels Model

A third alternative transport process using the similar fundamental ideas from the above models have been developed from motorized vessels on water. The research of re-aeration from motorized boats originally came about to evaluate the re-aeration impact from high volume of traffic through a particular water body. This re-aeration process of motor vessels may be a rough estimate of a hydraulic dredge motor mixing process particularly in mixing water at the bottom of the water column. When hydraulic dredging occurs, the ladder stirring the bottom waters primarily makes the turbulent movement of water. It forms large turbulent eddies similar to those surrounding a large vessel.

As a boat moves through shallow waters, the surface and bottom waters are displaced. This creates a flow-like movement of water along the sides and bottom of the boat. In this regard, the action is very similar to the cutterhead/auger dredge in its displacement of water

by the swing motion of the ladder through the water. A slow turnover is less noticeable at the surface, especially at larger depths, due to the turbulent force dissipating near the bottom; high flows occur in shallow waters. However, eddies on a large scale slowly reach the surface to create a continuous turnover of chemically depleted water and replacement with concentrated-bulk waters.

Estimates for the mass transfer coefficients of large and small motor vessels have been made through both laboratory and field studies. A set of experiments was designed to test the effects of both small and large vessels on the reaeration coefficient based on the number of passes through the water (Thibodeaux et al. 1994). Approximate values can be estimated by relating the number of passes of the vessel to the passing of the hydraulic dredge arm swing motion through the surface waters. In the case of small vessels, 1 to 2 cm/hr values were found to cover a range of 1 to 20 passes per hour with a variation in vessel motor power from 14 W to nearly 300 W. For larger vessels with a range of power from 50 W to 1000 W, the MTC was found to remain similar to the small vessels with a range of 1.3 to 2.8 cm/hr.

3.1.3 Chemical Flux

3.1.3.1 Enclosed Flowing Stream

3.1.3.1.1 DOU

Dredging of rivers or streams is often performed using some form of enclosure mechanism such as a silt curtain. They reduce the particle concentration downstream from the dredge site minimizing losses by evaporation. For the case of modeling an enclosed section of a river, the assumption is made that a negligible number of suspended solids exited the DOU. This condition results in downstream emissions primarily from chemical in

solution leaving the DOU area. The MTCs are broken down into two zones: forced convection and natural convection. For the natural zone within in the enclosed area of a flowing river, the emissions are not enhanced by dredging activities. Outside the enclosed area, the downstream plume concentration is influenced only by natural convective mass transfer. The forced convection zone refers to the emission area surrounding the dredge, which is enhanced by dredge-generated turbulence. These two zones are shown in detail in Figure 3.2. The descriptions of these zones are detailed in Section 3.1.2.

The forced zone has an increased TSS concentration level relative to the natural zone. Outside of this region, the second zone has significantly lower TSS levels. Both zones in the DOU are assumed well-mixed sections. Personally communicated suggested TSS levels by Paul Schroeder (Feb. 05) are listed in Table 3.1. Beyond the DOU area, water exits with a finite concentration of chemical in solution. This downstream area is assumed to have even smaller TSS concentration with a negligible result on emissions of this zone. Natural convection processes including the wind and the hydraulic flow effects on the interfacial resistance govern the emissions from the downstream section from the DOU. It is assumed that primary source of chemical concentration for emissions are the chemical in solution. Although the most common containment mechanism is by silt curtains, sheet pilings can also be constructed for containment walls to the DOU. In the case of metal sheet piling, no chemical flow occurs past the boundary and chemical flux downstream is excluded from the evaluation of emissions.

Table 3.1 Convective Zone TSS Concentration Levels

Location	TSS Concentraiton (gm/L)
DOU Forced Convective Zone	~500
DOU Natural Convective Zone	~50
DS Natural Convective Zone	~0

Using the mass transport descriptions and equations of Section 3.1.2, the application to estimating the chemical flux from the dredge site will involve using a mixed tank mass balance on the DOU with a plug flow balance for the exponential concentration decay downstream of the DOU. The in-solution concentration in the forced convection (FC) zone is:

$$\rho_{A2FC} = \frac{w_a}{K_{A32} + \frac{1}{\rho_{32FC}}} \tag{3.6}$$

where: w_a = chemical loading concentration on bed sediment

ρ_{32FC} = suspended solid concentration

K_{A32} = sediment-to-water partition coefficient

Similarly for the natural convection (NC) zone:

$$\rho_{A2NC} = \frac{w_a}{K_{A32} + \frac{1}{\rho_{32NC}}} \tag{3.7}$$

These concentrations are used in the following equations for estimating the flux from the two zones by:

$$n_{ADOUNC} = {}^{1}K'_{A2NC} (\rho_{A2NC} - \rho^*_{A2}) \tag{3.8}$$

and

$$n_{ADOUFC} = {}^{1}K'_{A2FC} (\rho_{A2FC} - \rho^*_{A2}) \tag{3.9}$$

where: $\rho_{A2`}$ = background chemical concentration in air

${}^{1}K'_{A2}$ = overall water-to-air mass transfer coefficient

In determining the separate flux estimations for the DOU, the overall flux can be determined based on the area of the forced convective zone (A_{FC}) and overall area of the DOU (A_{DOU}).

$$n_{ADOU} = \left(1 - \frac{A_{FC}}{A_{DOU}}\right) \cdot n_{ADOUNC} + \left(\frac{A_{NC}}{A_{DOU}}\right) \cdot n_{A.DOUFC} \tag{3.10}$$

After estimating the overall flux from the DOU, the estimation for the downstream chemical concentration, ρ'_{A2NC}, is made using the following equation:

$$\rho'_{A2NC} = \left(\rho_{A2NC} - \rho'_{A2}\right) \cdot \exp\left(\frac{-'K'_{A2NC} \cdot \tau}{h}\right) + \rho'_{A2} \tag{3.11}$$

As shown in the above equation, the parameters used in these equations are based on that at the exit DOU boundary. Since this section by the DOU exit is primarily natural convection and well mixed, these parameters are used in calculating the downstream chemical concentration. This discussion is further explained in Section 3.2.

The variables on the RHS of Equation 3.11 are designated for the natural convective zone inside the DOU. The chemical emissions are estimated by using the MTC for the natural convective zone along with the concentration evaluated using Equation 3.11.

$$n_{ADS} = {}^{1}K'_{A2NC} \left(\rho'_{A2NC} - \rho^*_{A2}\right) \tag{3.12}$$

where the background concentration, ρ^*_{A2}, over the entire river is assumed to be zero.

3.1.3.1.2 Barge

On calculating this flux, an additional source term incorporating the emissions from the barge usually located just outside the DOU must be added into the calculation to the forced convective flux. This is added into the forced convective flux since the dredged material on the barge will be comprised of a layer of standing water with high concentrations

of TSS and a contaminated source sediment bottom which is representative with the conditions in the forced convective zone. In assuming these two zones are equivalent, the area of forced convective emissions will be increased by the surface area of the barge.

3.1.3.2 Flowing River Without Enclosure

The case of dredging commencing in a river without an enclosure can be modeled similarly as the case of an enclosed unit of the river. This model essentially involves emissions from a DOU area comprised solely of the forced zone convection and a downstream plume of emissions. The chemical flux for the forced convective zone will be handled identically the same as in the enclosed river using Equations 3.6 and 3.9. The downstream plume must be handled differently from the enclosed river model because of suspended solids in the natural convective zone moving downstream of the forced zone will have an effect on the overall emissions. It will be comparable to the ponded CDF model to be discussed in Chapter 5. The natural convective zone will use the methods developed for the ponded scenario to estimate the chemical concentration moving downstream. This concentration will be used to calculate the flux from the natural convective zone using Equation 3.8. Once the natural zone flux as a function of distance is determined, it must be integrated and divided by the A_{NC} to estimate the average flux from the downstream plume. The downstream flux can then be added to the DOU flux for an overall estimate of the chemical flux to air.

3.1.3.3 Enclosed Embayment

The chemical flux from a DOU within an embayment involves a modification to the concentration term since the chemical is undergoing diffusion from turbulent waters generated by wind rather than hydraulic flow. The area inside the radius of the forced

convection zone, r_o, is comprised of a uniform chemical concentration in solution, ρ_{A2}. The dispersion process is modeled as occurring in a radial direction from the center-forced zone as shown in Figure 3.3.

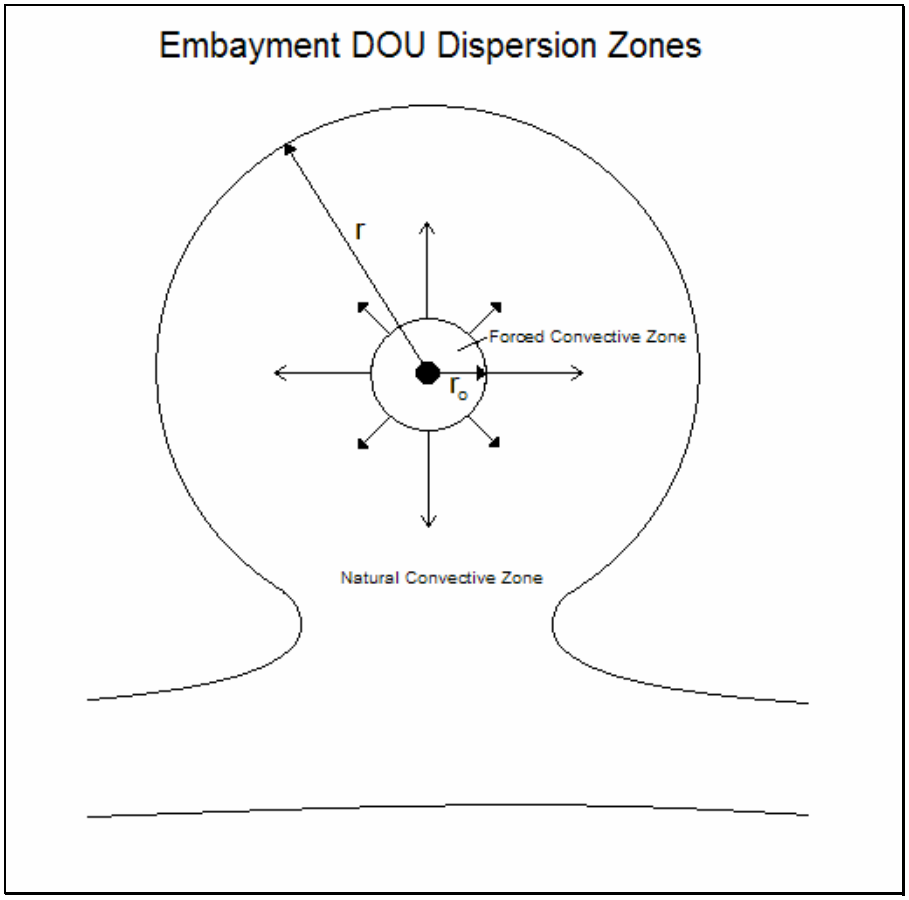

Figure 3.3 Radial Chemical Dispersion in Embayment Waters

A steady state mass balance was developed to describe the chemical dispersion in the x and y direction including a generation and loss term from sediment and evaporative flux, respectively. The concentration used in the volatilization flux equation is determined through the superposition of the concentration from dispersion and evaporation from the dredge forced zone onto the steady state chemical concentration, ρ_{A2SS}, generated from the

bed. In developing an expression for the chemical concentration, the mass balance of chemical A around the dredge involves the sediment flux being incorporated into ρ_{A2SS}.

$$\frac{d^2}{dr^2}\rho_{A2} + \frac{1}{r}\cdot\frac{d}{dr}\rho_{A2} - \frac{'K'_{A2}}{D_{A2y}}\cdot\rho_{A2} = 0 \tag{3.13}$$

The background concentration is approximated as zero in order to approximate this concentration. This resulting chemical concentration is:

$$\frac{\rho_{A2}(r) - \rho_{A2SS}}{\rho_{A2FC} - \rho_{A2SS}} = \frac{K_o\left[\left(\frac{'K'_{A2}\cdot r^2}{h\cdot D_{A2y}}\right)^{0.5}\right]}{K_o\left[\left(\frac{'K'_{A2}\cdot r_o^2}{h\cdot D_{A2y}}\right)^{0.5}\right]} \tag{3.14}$$

The forced convective concentration can be determined as expressed in Equation 3.6. The horizontal diffusivity of the chemical, D_{A2y} (ft^2/s), can be estimated by the following equation from Thibodeaux L. J. (1996):

$$D_{A2y} = 0.0125\ r^{4/3} \tag{3.15}$$

where: r = radial distance of the plume/embayment from the forced zone (m).

3.1.4 Estimating Areas within the DOU

The area of the DOU, A_{DOU}, is broken into two parts; the forced convective area, A_F, and natural convective area, A_N. Evaluating the total and convective area is required for the calculations of mass transfer coefficients and mass evaporative rates. The A_F is impacted directly by the mechanical device. Estimates of the forced convective area can be determined by:

$$A_F = (17\ ft^2/hp)\cdot P \tag{3.16}$$

where: P is the delivered power (hp) for >13.5 hp

The natural convective area is determined by taking the difference between A_{DOU} and A_F. For this computation, the A_{DOU} is case dependant.

$$A_N = A_{DOU} + A_F \tag{3.16}$$

The total enclosed stream for case area is determined by silt curtain or containment area design conditions if known or by estimating the size. For the Non-Enclosed Flowing Stream case, the DOU area consists of only of the forced convection zone.

For the case of Embayment Waters, the area for evaluation of chemical emissions can be estimated by back solving for the area using the following approach. By gathering the concentration terms to the LHS, a fraction of decreased concentration from the source, f, can define the ratio of the modified Bessel function of the second kind (K_o).

$$[(\rho_{A2}(r) - \rho_{A2SS}) / (\rho_{A2FC} - \rho_{A2SS})] = f \tag{3.17}$$

This fraction is used in estimating the area of the DOU. The A_{DOU} is estimated as the area within the radius of $\rho_{A2}(r)/\rho_{A2}(r_o) = 10\%$, where this point marks the radius, r, outside the forced area which contains a soluble chemical concentration which is 10% of that concentration in the forced convective zone. This evaluation can be made by setting f = 0.1 and then back-calculating the radius. The concentration fraction can be changed to a desired value depending on the requirements on the model.

$$f = K_o(({}^1K'_{A2}\, r^2 / h\, D_{A2y})^{1/2}) / K_o(({}^1K'_{A2}\, r_o^2 / h\, D_{A2y})^{1/2}) \tag{3.18}$$

This radius can then be determined numerically and used in estimating the area of emissions, A_{DOU}. Numerical solutions for the modified Bessel function of the second kind are given in Table 3.2 (MathCAD generated results).

Table 3.2 Numerical Values for Modified Bessel Function of the Second Kind

r	$K_0(r)$	r	$K_0(r)$	r	$K_0(r)$	r	$K_0(r)$	r	$K_0(r)$
0.1	2.43	2.1	0.101	4.1	9.98E-03	6.1	1.12E-03	8.1	1.32E-04
0.2	1.75	2.2	0.089	4.2	8.93E-03	6.2	1.00E-03	8.2	1.18E-04
0.3	1.37	2.3	0.079	4.3	7.99E-03	6.3	9.00E-04	8.3	1.07E-04
0.4	1.11	2.4	0.070	4.4	7.15E-03	6.4	8.08E-04	8.4	9.59E-05
0.5	0.92	2.5	0.062	4.5	6.40E-03	6.5	7.26E-04	8.5	8.63E-05
0.6	0.78	2.6	0.055	4.6	5.73E-03	6.6	6.52E-04	8.6	7.76E-05
0.7	0.66	2.7	0.049	4.7	5.13E-03	6.7	5.86E-04	8.7	6.98E-05
0.8	0.57	2.8	0.044	4.8	4.60E-03	6.8	5.26E-04	8.8	6.28E-05
0.9	0.49	2.9	0.039	4.9	4.12E-03	6.9	4.73E-04	8.9	5.65E-05
1.0	0.42	3.0	0.035	5.0	3.69E-03	7.0	4.25E-04	9.0	5.09E-05
1.1	0.37	3.1	0.031	5.1	3.31E-03	7.1	3.82E-04	9.1	4.58E-05
1.2	0.32	3.2	0.028	5.2	2.97E-03	7.2	3.43E-04	9.2	4.12E-05
1.3	0.28	3.3	0.025	5.3	2.66E-03	7.3	3.08E-04	9.3	3.71E-05
1.4	0.24	3.4	0.022	5.4	2.38E-03	7.4	2.77E-04	9.4	3.34E-05
1.5	0.21	3.5	0.020	5.5	2.14E-03	7.5	2.49E-04	9.5	3.01E-05
1.6	0.19	3.6	0.017	5.6	1.92E-03	7.6	2.24E-04	9.6	2.71E-05
1.7	0.17	3.7	0.016	5.7	1.72E-03	7.7	2.01E-04	9.7	2.44E-05
1.8	0.15	3.8	0.014	5.8	1.54E-03	7.8	1.81E-04	9.8	2.19E-05
1.9	0.13	3.9	0.012	5.9	1.39E-03	7.9	1.63E-04	9.9	1.97E-05
2.0	0.11	4.0	0.011	6.0	1.24E-03	8.0	1.46E-04	10.0	1.78E-05

3.2 Model Applications

The focus of this section is to verify whether the model produces reasonable estimates using sample input parameters. The following section is **not** designed to provide actual results. These input values were estimated to evaluate the profile output of the model. The variables listed as the inputs along with the output figures were developed for modeling emissions from a DOU along with the downstream section. The results appear in Figure 3.4.

The input values were estimated to evaluate the profile output of the model. Listed in the Appendix are the inputs values for the DOU emissions model for an enclosed river. These chemical properties were based on Naphthalene being the selected chemical. Some of the DOU parameters include a wind velocity of 9.26 mph, water flow-through of 0.5 m^3/s, surface area 1569 m^2, and a 300 hp dredge. Some of the concentrations include suspended solids in the forced zone set at 500 gm/L and 50 gm/L in the natural. The above equilibrium air concentration is assumed to be negligible.

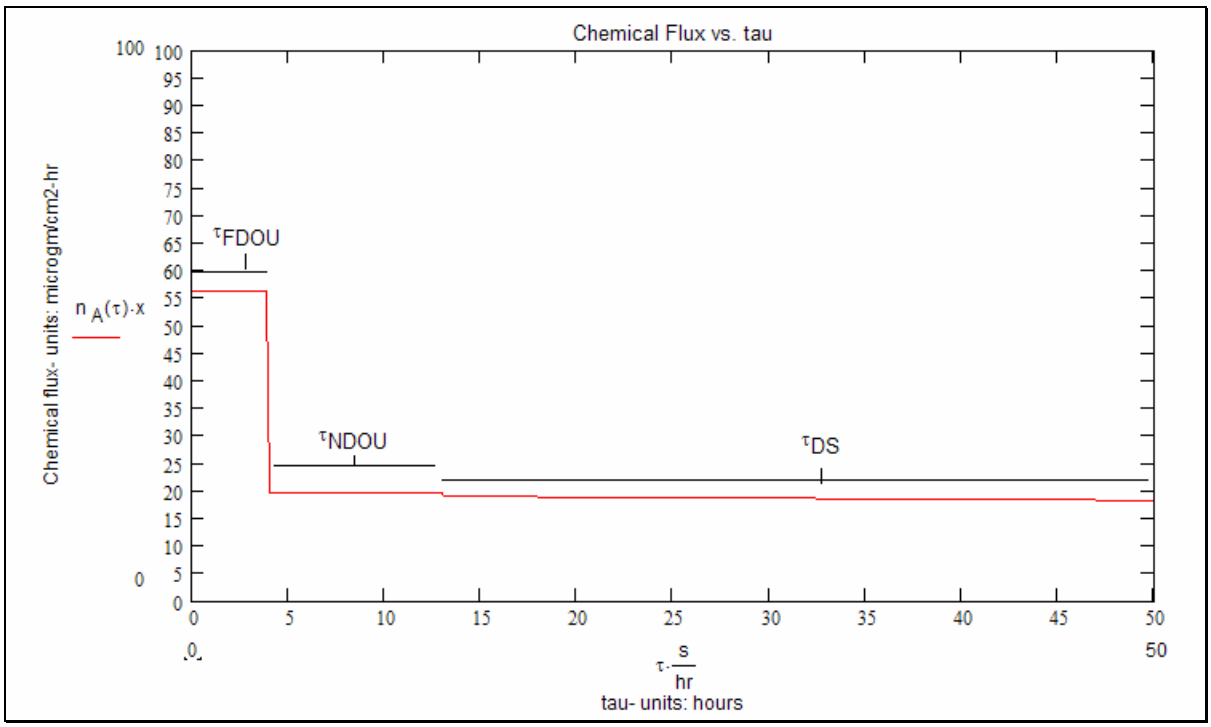

Figure 3.4 Chemical flux from DOU and Downstream of Enclosed River

Shown in the figure above is a typical emission profile from a DOU and downstream area of an enclosed river dredging process. The figure shows three sections of emissions as mentioned in the model discussion in previous sections; forced convective zone of DOU, natural convective zone of DOU, and natural convective zone of DS. The forced zone contains the highest level of emissions due to the increased suspended solids in this zone and the increase in mass transfer coefficient from the dredge. The next emission zone is the DOU natural convective area which is far lower primarily due to the decrease in mass transfer coefficient. The last emission zone contains those from the downstream area where chemical is released from the water column containing chemical in solution only due to elimination of solids from the containment device. This profile will change based on the settings used in the model. These results were used to provide a schematic of the model.

CHAPTER 4

EXPOSED DREDGE MATERIAL CDF EMISSIONS MODEL

This chapter consists of a self-contained report submitted to ERDC. The report was entitled: "PAH Volatilization From Dredged Material Under IHC/CDF-Like Conditions: Wind Tunnel Flux Measurements and Modeling" with authors Fountain, Thibodeaux, Valsaraj, 2005. 1769p.

4.1 Executive Summary

Volatilization rates of Naphthalene (NAPH), 2-Methylnaphthalene (M-NAPH) and Phenanthrene (PHEN) from Indiana Harbor Canal dredged materials (DM) were obtained from air samples taken in a large-scale (120 cm width x 460 cm length) soil lysimeter wind tunnel apparatus. For average loadings of 2.7, 1.2 and 4.3 mg/kg (dry soil) the maximum fluxes of 50, 25 and 2.0 ng/cm^2-h were observed for NAPH, M-NAPH and PHEN, respectively. These maximum values were observed at soil surface "drying times" of 425, 125 and 100 hours during three experiments conducted with a 1.2 m/s (2.6 mph) wind speed with air temperatures and relative humidity ranging from 3 to 25^{o}C and 50 to 90%, respectively. The experimental run times were 28, 15 and 40 days for experiments 1, 2 and 4, respectively. Data obtained from these experiments revealed some key features about chemical volatilization process from drying DM soil that are unique and contrast the process from normal and agricultural surface soils. Initially DM soils have very large water-to-solids ratios. Once placed in a Confined Disposal Facility (CDF) the mechanically dredged DM undergoes the combined processes of bed consolidation, water run-off and evaporation as the water content is reduced. These processes control the behavior patterns of the chemical flux

from the surface. Three chemical flux regimes were identified and used with traditional water and chemical evaporation theories to develop a chemodynamic emission model.

Traditionally the solids drying process has a constant water evaporation rate (i.e., flux) period followed by a falling rate. This pattern was not observed for the three-polyaromatic hydrocarbons (PAHs). Initially in Regime-0 the chemical flux is low to zero and controlled by a water layer covering the DM solids. Regime-I commences after the water layer is gone and the DM solids become progressively free of liquid water. The chemical flux progressively increases with time during this apparent constant rate water evaporation process. The maximum chemical flux is reached when the surface of the DM bed is completely dry. In Regime-II the chemical flux decreases with increasing time as its mass in the surface layers becomes depleted. Sampling of the DM surface solids showed the water content decreased and the air-filled pore space increased with time during Regimes-I and II. A depletion driven, falling chemical flux is a typical behavior pattern observed with normal and agricultural surface soils and this process has undergone much theoretical and laboratory study. As a result theory-based algorithms are available for quantifying the flux to air based on soil characteristics and chemical properties and atmospheric boundary layer transport parameters. This flux equation is the basic algorithm used in the "dry patches" model developed for chemical volatilization from the drying DM bed.

The dry patches model developed in this study applies to Regimes-I and II. Although relevant to other aspects of the overall CDF chemical emission inventory analysis, the Regime-0, or water ponded model, is the subject of a separate report. Once the water covering is gone Regime-I commences and water evaporation originates from the bed surface to produce areas of dry patches on the surface of the DM soil. Initially water-filled these

areas progressively become air-filled source areas for chemical volatilization. A linear increase in dry patch area growth with time was the relationship that best described the observed chemical flux vs. time behavior. Model drying time, t_D', established the completion time for the formation of new dry patch areas; in other words it marks the end of Regime-I. During Regime-II the recently formed and older surface patches increase in age with increasing time. Each patch undergoes chemical depletion as described above. The net chemical flux is the sum of the fluxes of the individual patches; it falls with increasing time and mimics the flux patterns observed for NAPH, M-NAPH and PHEN. The dry patch model appears to describe both the rising chemical flux in Regime-I and the falling flux in Regime-II along with the position of the maximum flux that defines the transition point. In essence the "dry patch" model contains two parameters, which quantifies the chemical flux vs. time behavior from drying DM solids placed in a CDF or similar setting. The two parameters are a linear time-patch growth relationship and the Regime-I drying time t_D'.

Two artifacts of the lysimeter-wind tunnel (L/WT) studies were unique to its operation and do not directly translate to DM field operations. Both stem from the Regime-0 water layer formation and disappearance. First, the bed mixing and consolidation process forces water upward for pond creation and increased moisture on the DM surface. This prolongs the drying time of Regime-I. Second, the development of a "dirty" water layer on the DM followed by its evaporation, deposits a thin solid layer with elevated chemical concentrations on the bed surface. This surface deposit produces enhanced chemical fluxes so that the model generated fluxes required correction factors to account for the observed ones. In the field, water produced by bed consolidation is allowed to run-off without the formation of localized ponded areas so that both artifacts do not materialize. In the field

much shorter surface drying times and no elevated surface concentrations are expected. Such drying actions were found to differ in the discussed model experiments compared to the ERDC Vicksburg/IHC DM "field" experiment (Ravikrishna et al., 2001). The experiments in creating the discussed model closely matched that of the "field" experiment except for the drying process found in the sediment bed. This process differed due to the field study apparatus was designed to drain water through the bottom of the flux chamber. With the runoff and drainage of the water in the chamber along with evaporation, the bed pore space volume quickly changed from air-filled to water-filled. This bed drying action is critical to this model in that it regulates how quickly pore space becomes filled with air and allows quick transport to the surface for emissions. The results from this field experiment showed a sharp decline in chemical flux before as it exponentially decayed. These results differed from that in the wind tunnel by making the dry time insignificant as the surface sediment driving emissions became dry instantaneously. Notwithstanding these artifacts, the L/WT experiments provide new insights into the chemical volatilization process from DM and a focus for the development of a simple model, which captures both the qualitative and quantitative aspects of the chemodynamics. The report contains a discussion of these artifacts and presents other guidelines for translating and applying the dry patches model in the field

4.2 Introduction

The objectives of the investigations were to obtain data and develop a science-based volatilization process model for soil-to-air chemical emissions from dredged materials (DM). Wind tunnel volatilization experiments using Indiana Harbor Canal DM were conducted to produce data for modeling efforts. Most chemical evaporation data (i.e., flux to air) is

derived from soil-like sources and is based on laboratory experiments (Thibodeaux et al., 2002). Typically the equipment employed used small mass quantities, small evaporative surface areas, and contained soils not of dredged material origin. With one exception, all were laboratory scale evaporation experiments. The experiments in creating the discussed model closely matched that of the "field" experiment except for the drying process found in the sediment bed. Large-scale lysimeter/wind tunnel (L/WT) experiments appear to be the best compromise between the laboratory scale simulations and field scale measurements. The large evaporative surface areas and DM mass contained within the wind tunnel allowed close 1-to-1 mimicking of the drying/consolidation/cracking/etc. processes that occur in the field. In addition the L/WT apparatus has the advantages over the field in the ability to control the wind conditions and the air sampling to make precise measurements of water content, water losses, surface area of cracking and other tactics of the chemical flux measurements. Employing the IHC DM as the contaminant source material will provide critical data needed for estimating emissions at this particular site. This in turn will provide the understanding and the parameter quantification key to developing a more realistic chemical flux model. The two key objectives of this research are to: 1) obtain field-like chemical flux measurements for IHC/CDF dredged material and 2) update the existing USACE commissioned emission flux model (Thibodeaux, 1989) which was recently re-revised.

4.3 Background

As established in a recent literature review of models and data considerable information is available discussing the evaporative chemical release process from soils (Thibodeaux, et al., 2002). The fundamental theory of the process is well established and generally verified by numerous sets of data. Essentially it is a process that begins within the

chemical sorbed to the solid phase of the DM. Here chemicals desorb into the adjoining air-filled pores characterized by the air equilibrium desorption partition coefficient (H_ρ/K_{A32}); this is Step 1. The effective chemical diffusion coefficient in the vapor-phase of the porous media, quantified by D_e, moves the chemical to the air-soil interface; this is Step 2. The last transport step (Step 3) is the chemical species moving through a thin boundary film on the airside of the interface before being mixed with bulk air currents in the atmospheric boundary layer. An equation based on the Lavoisier mass-balance principle connects the flux, n, and the average chemical concentration, C_s, in the soil column. The major remaining uncertainty appears to reside with Step 2, diffusion of chemical vapor molecules through the open pores of the soil.

It is well known that the fraction of air porosity, ε_1, is a key variable in regulating the effective diffusion coefficient, D_e. The Millington-Quirk correction, which is $D_e^{4/3}$, is commonly used to modify the molecular diffusivity for the presence of the solid particle blocking and tortuous pathways. Typical agricultural soils behave ideally because they maintain rather uniform ε_1 values so that a constant D_e can be used for predicting pesticide and volatile hydrocarbon emissions. Due to the high initial water contents and large clay fractions DM soils appear to behave very non-ideal. One field-scale test using IHC DM displayed an emission-to-air behavior that could not be quantified by a constant D_e as typically used in these models (Ravikrishna et al., 2001). Post experiment analysis suggested that a complex behavior of ε_1 with time was the likely factor. It was hypothesized that the observed flux behavior was the result of water evaporation and the simultaneous volume shrinkage of the DM column (i.e., consolidation). Surface cracks were noted to appear early

on in the evaporation process. A critical review of this first field test appears elsewhere (Thibodeaux L. J. 2003).

4.4 Experimental Procedure

4.4.1 Wind Tunnel Design

A wind tunnel constructed at ERDC Vicksburg, MS was designed based on one used to measure selenium volatilization from soils (Dungan, et al. 2000). A lysimeter of dimensions height 0.46 m (1.5 ft) x width 1.22 m (4 ft) x length 4.57m (15 ft) designed to simulate surface water runoff (Price et al. 1996) was used as the base of the wind tunnel. A rectangular tunnel of height 0.91 m (3 ft) x width 1.22 m (4 ft) x length 4.57m (15 ft) open at each end was placed on top the lysimeter. It contained window panels along one side and topside in order to gain access and to view the inside of the tunnel. The soil-filled lysimeter served as the bottom-side of the wind tunnel. A schematic of the tunnel is shown in Figure 4.1.

An 11.2W (15hp) blower was used to draw outside air into the WT, which enters via an aluminum duct located outside the building with the opening at a height 4.57m (15 ft) above the ground. Once in the entrance zone the air stream is straightened and the flow evenly distributed using a 3-part section consisting of a honeycomb, a baffle, and screens. The baffle was made of sheet plywood with teardrop shaped holes to better distribute the inlet airflow arriving in the duct. A thin aluminum sheet of honeycomb cells 1.27 cm (½ in) X 15.2 cm (6 in) length was added to further straighten the flow. A stack of four wire screens were placed last to further assist in shaping the velocity profile over the lysimeter. Velocity profiles within the tunnel were measured using hotwire and impellor anemometers at locations of 1.22 m (4 ft), 2.44 m (8 ft), and 3.66 m (12 ft) from the entrance screen.

Air sample collection apparatuses were located both within the tunnel section and in the exit section outside of the tunnel. A thin circular metal disk angled at 45 degrees to the wind and placed 30 cm upstream the sample device was the "mixing body" used to homogenize the air stream (Ruscheweyh, 1984) prior to sampling. This gas mixing system has been shown to be very effective in producing uniform concentrations in converging gas streams. The blower unit is located a few feet beyond the air sample port. The air exits at a height of 9.14m (30 ft) above the ground.

4.4.2 Wind Speed and Profile

The stack of devices installed in the L/WT inlet section, consisting of baffles, honeycombs, and screens shaped the airflow above the soil surface in an attempt to conform it to field like conditions. Measurements taken in the 30 cm region above to soil displayed the turbulent boundary layer profile shape with friction velocities and surface roughness heights commonly found at field sites. These results gave evidence that the chemical transport processes in the air boundary layer above the soil were realistic simulations of field conditions.

4.4.3 Dredge Material Source

Sediment samples from five separate reaches of the IHC were collected in July of 2003. The objective of sample collection was to obtain sediment samples representative of the material to be dredged in regards to location, quantity, and amount of contamination. A total of 15 55-gallon (200 L) metal drums were filled with sediment and shipped to ERDC Vicksburg in a refrigerated truck (Saichek, 2003). All containers were stored in a refrigerated trailer (4^{o}C) until ready to be mixed.

4.4.4 Sediment Handling and Analysis

The DM solids had consolidated during transportation and storage time and significant amounts of water accumulated at the top of each container. Motorized propeller mixers were used to homogenize the drum contents before the material was transferred to the lysimeter where further mixing was conducted to homogenize all 15 drums. One 55-gallon drum was removed for use in plant up-take studies. Once filled, the sediment was raked evenly to form a uniform (3 to 4 cm) surface.

Five separate samples were taken from the homogenized dredged material in the lysimeter and analyzed for physical and chemical parameters (Table 4.1). Initial sediment contaminant concentrations for PAHs and PCBs were determined by GC/MS analysis (EPA method 8270) and GC analysis (EPA method 8082), respectively (Appendix II). Once mixed, the lysimeter was moved into a temperature-controlled building housing the wind tunnel (~23-25^{o}C). The sediment was covered with a thick layer of black plastic and the wind tunnel was lowered onto the lysimeter and sealed using gasket material and numerous bolts.

4.4.5 Experimental Methodology

A series of four experimental runs were initiated the following day. The plastic was removed from the sediment surface and the sediment was raked again to a uniform consistency. A soil temperature probe (Campbell Scientific, Logan, Utah) was inserted into the dredged material approximately 1 inch in depth from the sediment surface. Soil water content reflectometers (Model CS616) (Campbell Scientific) were inserted in the middle section of the wind tunnel 12 inches, 6 inches, and 1 inch below the sediment surface. Soil temperature and moisture were collected on a CR200 data logger (Campbell Scientific)

during the course of each experimental run. Wind speed, air temperature, and relative air humidity in the wind tunnel were monitored during each run using sensors obtained from Texas Instruments, Dallas, TX. Data was collected and recorded on a Solus data logger (Texas Instruments). All probes and sensors were removed prior to each new run to enable water addition and sediment remixing and replaced in the same location in the wind tunnel.

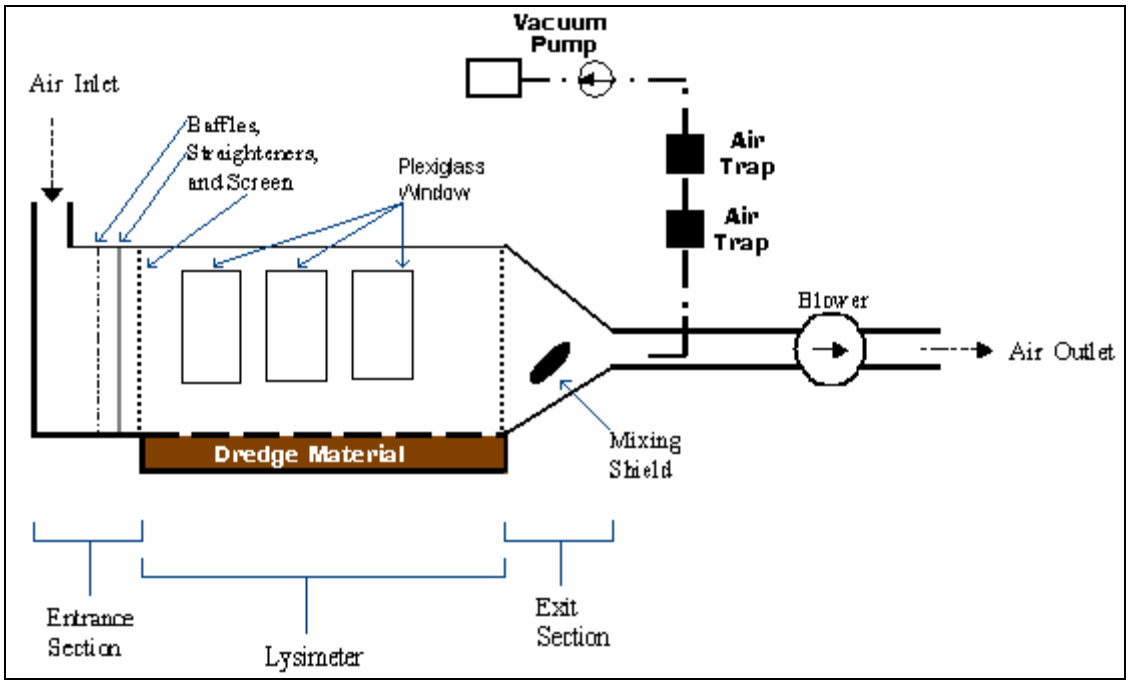

Figure 4.1 Wind Tunnel Schematic

In the first experimental run a representative air sample of the main air stream was collected on contaminant specific air sampling tubes (Orbo 44, Supelco, Inc.,) located in a separate chamber outside the wind tunnel (Figure 4.1). Air was pulled through the sampling tubes at a rate of 1.7 L/min using a GAST vacuum pump. This rate was selected based upon trap capacity specifications. Samples were collected continuously and removed at sample times of 6 hours, 3 days, 7 days, 13 days, 21 days, and 28 days after air was supplied across the sediment surface. Inlet air concentrations were periodically measured and determined to

be free of the contaminants of interest. The traps were solvent extracted and analysis for PAHs and PCBs were preformed according to EPA method 8270 and 8081.

Prior to the beginning of experimental Run 2, 30 liters of water were added to the sediment in the wind tunnel and mixed to approximately 1 foot in depth. The sediment surface was again smoothed and measurements were taken to determine unevenness of the material throughout the tunnel. In order to increase trapping capacity and raise sample detection limits, larger traps were constructed of the same material as the Orbo 44 traps (Supelpak-2). Air was pulled through these larger traps at 10 L/min. Samples were collected both outside and inside the wind tunnel to draw a comparison between sampling techniques in both locations. Samples were collected 2 days, 5 days, 9 days, and 15 days after air was supplied across the sediment surface. Traps were extracted and analyzed as stated previously.

A third run was initiated after adding 279 liters of water to the dredged material. Sediment was mixed to approximately one foot in depth. The run was discontinued after a sampling error was detected; all analytical results were below detection limits.

A fourth and final run using the larger traps as described in run 2 was initiated immediately following run 3. A total of 242 liters of water was added and mixed into the sediment. The sediment had consolidated and mixing was conducted to approximately 8 to 12 inches in depth. The sediment surface was again smoothed to prevent as much unevenness in the surface as possible. Samples were collected 2, 5, 9, 13, 19, 26, 33 and 40 days after air was supplied across the sediment.

4.5 Experimental Results

The primary observable from the L/WT apparatus was the chemical flux to air from the DM mass. From measured mass (ng) quantities collected onto adsorbent traps the exit concentrations in air, C_A (ng/m^3), of selected chemical species were obtained. The volumetric airflow rate, Q_1 (m^3/s), was measured as well. From these measured quantities the chemical flux to air, N_A (ng/m^2·h) was obtained from

$$N_A = Q_1 C_A / A \tag{4.1}$$

The measured fluxes for the three chemicals appear in Figures 4.2-4.4.

Due to the low chemical loading levels in the collected IHC DM, only naphthalene, 2-methylnaphthanlene, and phenanthrene fluxes were quantifiable. Collected mass quantities for other PAHs were too low or too few in number to be useful. Three successive experimental runs were performed in order to capture the variations of the flux

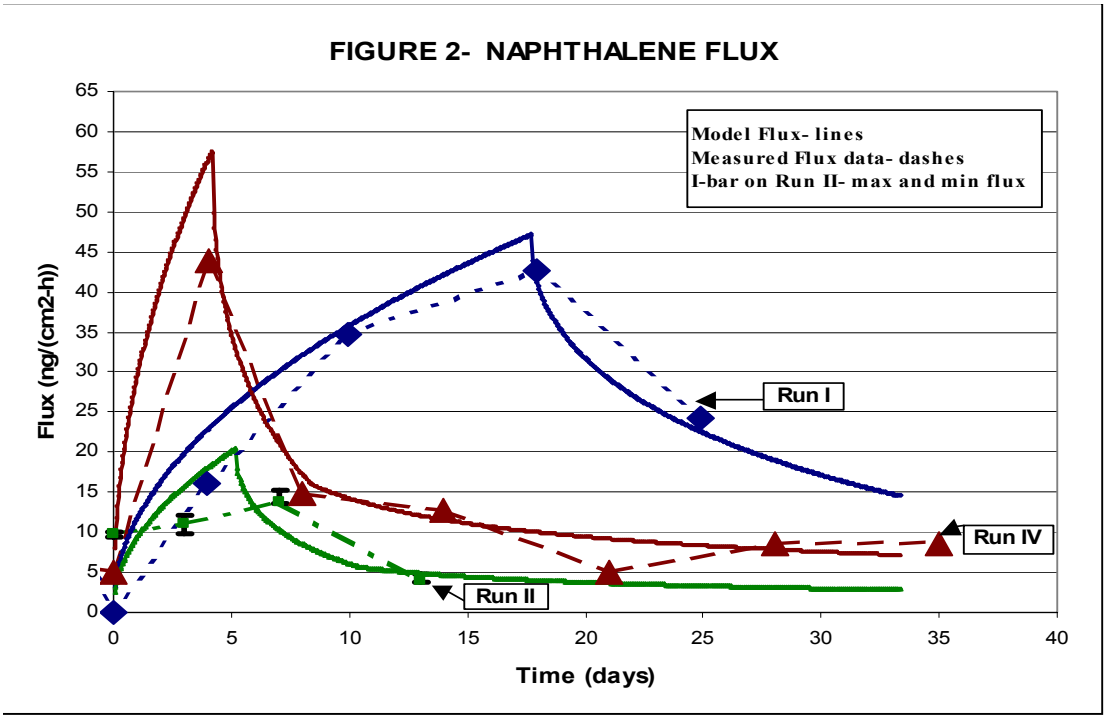

Figure 4.2 Naphthalene Measured Flux Data vs. Model Estimated Fluxes

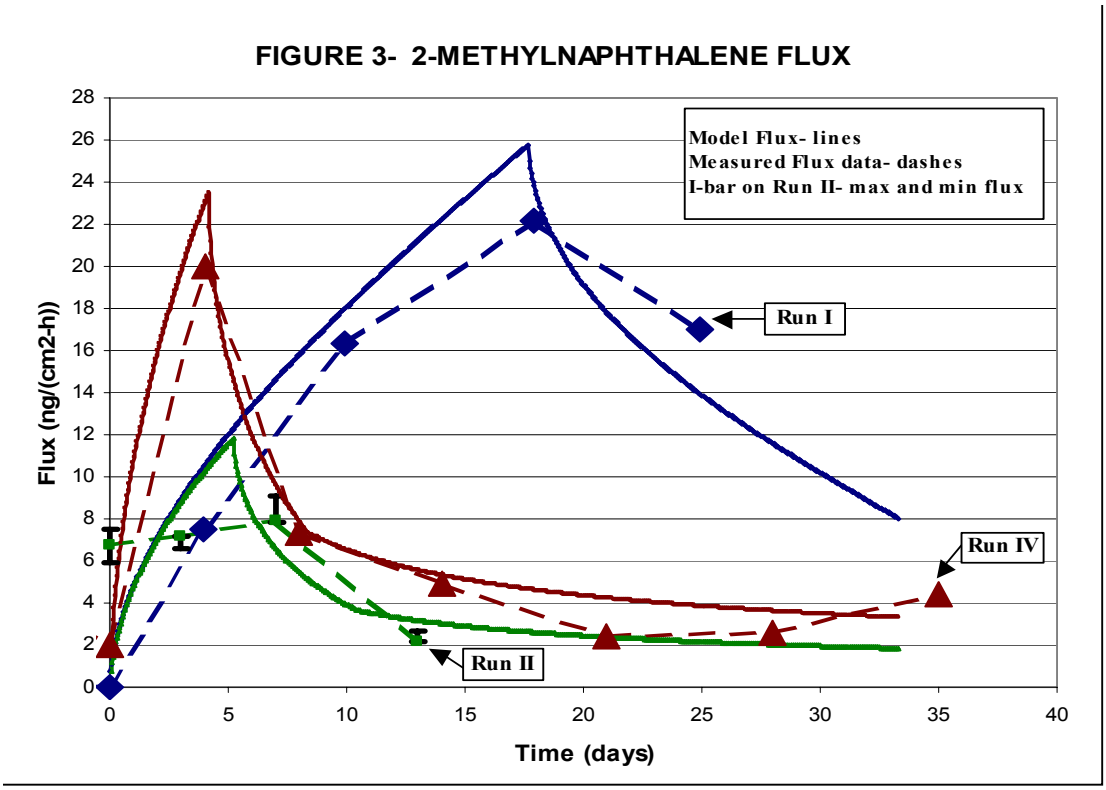

Figure 4.3 2-Methylnaphthalene Measured Flux Data vs. Model Estimated Fluxes

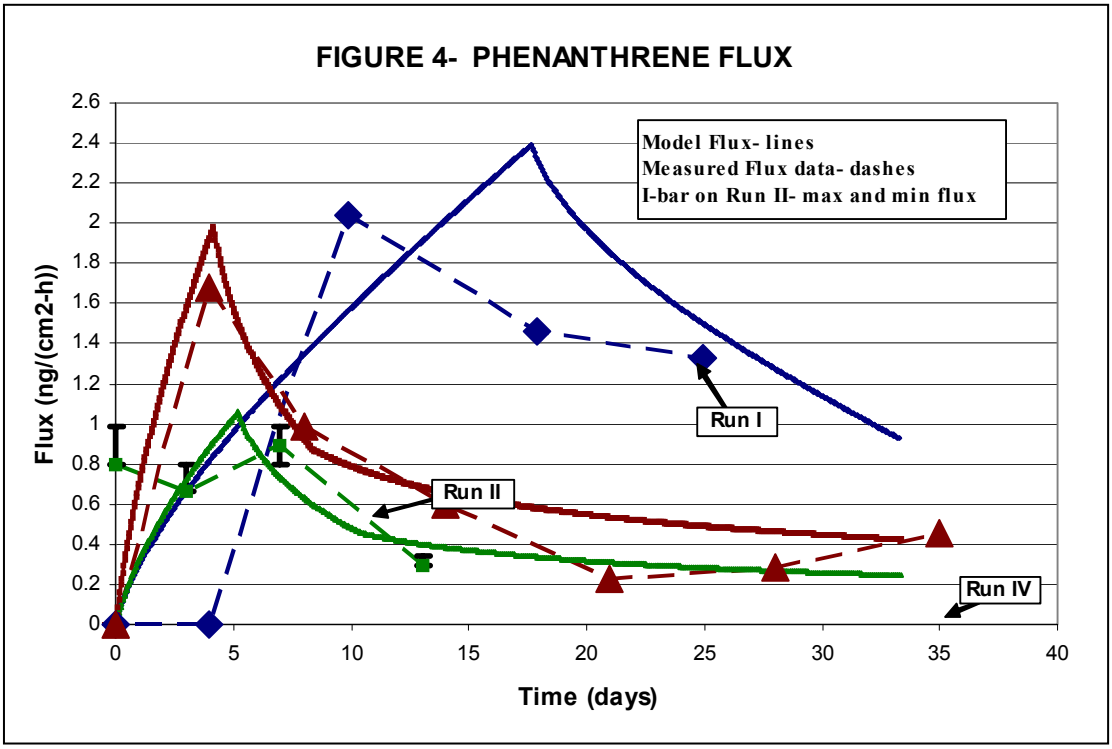

Figure 4.4 Phenanthrene Measured Flux Data vs. Model Estimated Fluxes

measurements. The experimental run-times were 670 hours (28 days), 360 hours (15 days), and 959 hours (40 days) for Runs 1, 2, and 4 respectively. The flux data for NAPH, M-NAPH, and PHEN displayed the same general trends with time. Fluxes for NAPH varied between 0 and 50, those for M-NAPH varied between 0 and 25 and PHEN fluxes ranged from 0 to 2 $ng/m^2 \cdot h$. Sample time intervals varied for each run; early-on six hours was used. However, as air concentrations decreased the sample collection time intervals were extended to 48 hours and 96 hours with some requiring 194 hours (8 days) in order to obtain measurable quantities on the adsorbent traps. In addition to NAPH, M-NAPH and PHEN, small quantities of acenaphthalene were observed. Occasionally, even smaller quantities of pyrene and fluorene near the detection limit of < 0.10 μg/ml were noted. However, the data associated with these low levels were judged to be unreliable for flux interpretation purposes. The data on these and other PAHs appear in Appendix II. The following paragraphs provide an explanation for the time-behavior patterns for the observed NAPH, M-NAPH, and PHEN fluxes; focusing on NAPH due to the higher chemical fluxes.

4.5.1 Run 1

As Run 1 commenced, 2.6 m^3 of DM was placed in the lysimeter. The air velocity was adjusted to an average of 1.16 m/s (2.60 mph). A ponded/soupy water layer existed on the surface of the DM initially. After a few days the ponded water was visibly absent. During this time period the NAPH flux was initially 21 $ng/m^2 \cdot h$, but decreased rapidly and values were below detection limits (<0.10 ug/ml) were observed after 72 hours (3 days), which marked the end of Regime-0.

Regime-I commences when the chemical flux resumes. It is assumed that the reappearance of the chemical flux is due to the formation of dry patches on the surface of the

DM. This process proceeds slowly because the bed solids continue to consolidate and free water is forced upward. Since water evaporation is faster than that forced-up ponded water does not develop on the surface. The majority of consolidation-produced water appeared to end on Day 7; it was reported that the overall surface was "beginning to dry". On Day 11, cracks on the surface of the DM became apparent. The chemical flux increased as water-free porous surface areas (i.e., patches) increased with time. The increasing chemical flux period is defined as Regime-I. Some water was observed at depth in the soil cracks indicating consolidation was still occurring on Day 15. The surface of the DM had receded from 2.5 to 3.8 cm below the top of the lysimeter. On Day 20, the sediment level had decreased 5.1 cm. This amounts to 228 liters of water evaporated from the lysimeter. The surface cracks were 1 to 1.2 cm in width and 2.5 cm in depth on Day 20 while 2 cm in width and 6-8 cm in depth on Day 26. On Day 21, the NAPH flux reached a maximum value of 49 ng/m^2-h. This marked the end of Regime-I.

The falling chemical flux period is defined as Regime-II. On Day 28, the final NAPH flux measurement was 28 ng/m^2-h. Soil moisture content measured on composite samples for Days 0, 12, 15, and 21 fell from 94 to 79, 62, and 55% respectively. In general these correspond to the observed water evaporation losses. Clearly, the solids consolidation process produces water, which travels upward since the bottom of the lysimeter is sealed; no leachate was collected or withdrawn. This water production process opens the soil pore spaces and affects the chemical flux to air. As introduced, these three regimes will be used to characterize the chemical and water behavior in the lysimeter: Regime-0 is the ponded period, Regime-I is the surface patches formation period and Regime-II is the dry surface period.

These water regimes influence the NAPH flux rate. The Regime-0 occurs early on after filling the lysimeter with DM; rapid solids consolidation produces ponded water on the surface. The second water regime, Regime-I, is characterized by less rapid consolidation, high water contents with continuing water evaporation. Relative dry soil surface patches and numerous cracks appeared on Day 14. Between Days 7 and 14 (approximately) the soil pore spaces increasingly contain air rather than water. At 25˚C, the chemical diffusivity for NAPH in air is 185 cm^2/h, where it is only 0.02 cm^2/h in water. Since the air-filled pores dominate the chemical transport within the soil the flux gradually increases over the period as shown in Figure 4.2 for Run –1. Soil temperature varied from 15˚C to 25˚C and % RH 65 to 90 over the period. Dry surface patch areas with air-filled soil pore spaces begin to appear at the end of Regime-0. In effect Regime-I is characterized by surface drying that converts a porous but water-filled DM soil surface to containing air filled surface patches. When the patches cover the entire surface the maximum chemical flux occurs and defines the time, t_D'. This marks the end of Regime-I and the start of Regime-II.

High water fluxes cannot be maintained once the surface is dry. This initiates the next water regime, Regime-II. Water depletion occurs from the upper soil layers but the diffusion path length increases with time. Since the quantities needed for evaporation originated well below the interface, the flux decreases. A dramatic decrease in flux occurred between Days 21 and 28. In summary, Regime-0 contains free-water on the surface, in Regime-I air-filled pore spaces gradually replace water-filled ones, and Regime-II represents full air-filled soil pore spaces and a cracked surface. The chemical flux pattern responds to the three water dominated regimes. Considerable bed consolidation occurs throughout Regimes I and II.

The flux vs. time behavior of M-NAPH and PHEN shown in Figure 4.3 & 4.4 are very similar to that of NAPH for Run-1. The three water regimes affect it as well. It is low when a ponded condition exists and increases as the water evaporation opens soil pores to achieve a maximum flux value. Upon reaching a maximum flux, chemical depletion from the dry upper layers precedes producing progressively lower fluxes to a low value on Day 28. The dramatic effect of chemical depletion with time is better appreciated in viewing the Run-4 data, which is also shown in Figures 4.2 and 4.3.

4.5.2 Run 2

At the end of Run-1, the airflow was stopped and approximately 30 liters of water was added and mixed into the surface soil to produce a uniform mud layer without a significant water layer. The wind speed was again set at 1.16 m/s (2.60 mph) while the soil temperature and relative humidity ranged as that in Run-1. On Day 6, the surface was still moist and cracks developed on Day 7. This cracking continued and by Day 15 several cracks had appeared (1-2 cm in width and 5 to 8 cm in depth). The experiment ended on Day 15. Four large cracks 2 cm wide by 8 to 11 cm in depth existed on the surface soil. The 30L of water did not replace the 228L lost during Run-1. A Regime-0 with ponded water never truly developed. Regime-1 characterized by dry surface patch formation was short lived. The maximum flux occurred at $t_D' = 7$ days. It took 16 days in Run 1. Figures 4.2-4.4 show data for NAPH, M-NAPH, and PHEN with increasing fluxes during this period as air replaced water in the pores. As time increased beyond t_D' the flux decreased; a value of 5 ng/m^2-h occurred on Day 11 for NAPH.

Replicate samples, n=3, at each sample time were performed on Run 2. The measured flux range appears in Figures 4.2-4.4 as a vertical bar at each time. The peak

fluxes were lower than those in Run-1 by approximately 70%. This occurrence of lower fluxes has no definite explanation at this time. Mixing in of the chemical depleted surface layers may have produced a lower soil concentration and in-turn lower fluxes are manifested. Because insufficient water was added, the peak flux value may have been missed during sampling. The maximum may have occurred between Day 5 and Day 9. Nevertheless, this short time-period experiment displayed some of the same patterns observed with Run-1. The turnaround time between Run 1 and 2 occurred in a single 24-hour period, 23-24 October 2003. The DM mass in the lysimeter was not returned to its initial water content. Soils at depth in the lysimeter were well consolidated during the twenty-nine days of Run-1; and not re-mixed with the surface layers. The top surface of the DM level in the lysimeter was down 13 cm when Run-2 started. In combination, these factors may have somehow produced the low fluxes.

4.5.3 Run 4

At the conclusion of Run 2, a more aggressive procedure was adopted for mixing-in water in an effort to return the DM mass to its initial water content and uniform consistency. Before Run-4 commenced another sediment re-wetting and re-working activity occurred. A total of 520 liters (0.52 m^3) of water was added in five batches and mixed into the soil. Some ponded water appeared on the surface after the mixing. This run was the longest of the three lasting forty days. Seven flux observations were made for NAPH, M-NAPH, and six for PHEN over the period; these appear in Figures 4.2-4.4 respectively. Although a full restoration of the DM to initial water conditions did not occur, it was sufficiently reconstituted that it displayed the three water regimes observed during Run-1.

At the start, the surface was wet and the average level was 10 cm below the top of the lysimeter. The DM had been in the lysimeter for four months (120 days) and the layers near the bottom of the 45 cm soil column were well consolidated and resisted break-up/re-wetting with the implements used for mixing. More aggressive water-soil mixing equipment may have damaged the bottom liner and resulted in water leakages. Initially, low fluxes were observed from the wet surface. Air temps ranged from 3.0^{o} to 12^{o}C and RH ranged 50% to 90%. Within two days, small cracks appeared on the surface. On Day 9, the cracks were 1-2 cm in width and extended 6-8 cm in depth. Air porosity was dominant in this now dry soil and the same magnitude of maximum chemical fluxes observed in Run-1 reappeared, but occurred much earlier in time. The maximum flux occurred on Day 9 for Run-4 whereas it occurred on Day 21 for Run-1. Soil drying occurred more rapidly in Run 4 because the DM mass commenced with less water than in Run 1.

The chemical flux vs. time behavior for Run-4 displayed an outstanding feature not previously observed. The flux dropped rapidly from the maximum and after approximately 10 days leveled off to what appeared to be near constant fluxes. These persisted for approximately 15 to 20 days. The final average soil surface level was 11.5 cm below the top of the lysimeter, down 1.5 cm from the start and displayed some degree of continuing consolidation. Soil cracks at the finish were 2.5 to 4 cm wide at the surface and extended 18 to 29 cm deep, however, the consolidation likely occurred in the top 10 to 15 cm reworked zone rather than at depth in the soil column.

The above discussion was dominated by the observations on NAPH and M-NAPH. In the opinion of the investigators, the flux measurements for NAPH and M-NAPH were more reliable than those for PHEN, which appear in Figure 4.4. The fluxes for PHEN were

roughly 10X lower than those for M-NAPH and 20 times lower than those observed for NAPH. Due to its low Henry's constant the measured fluxes for PHEN were low as expected even though it is present in the DM at the highest loading; see the C_S values in Table 4.1.

Table 4.1 Soil Parameters for IHC DM at 25C

Parameter	Units	Average	Minimum	Maximum
Organic Carbon Fraction	%	0.096		
Naphthalene	mg/kg	2.65	Undetectable	2.90
2-Methylnaphthalene	mg/kg	Undetectable	Undetectable	1.2 *
Phenanthrene	mg/kg	4.27	2.40	6.50
Acenaphthene	mg/kg	1.63	Undetectable	2.20
Fluoranthene	mg/kg	7.95	4.80	10.00
Fluorene	mg/kg	1.60	Undetectable	1.70
Pyrene	mg/kg	9.47	4.20	12.00
Particle density	g/ml	2.41		
Bulk density	g/ml	0.88	0.47	1.27
Air-filled porosity, ε_1	-	0.17	0	0.5
Moisture fraction	%	55.7	27.7	96

Small mass quantities were collected during air sampling and this challenged the detection limits of the chemical analysis. Because of these factors the flux data for PHEN was devalued and not used to adjust key model parameters. The final model was applied to PHEN and the data used in comparison because it represents chemicals with vastly lower Henry's constants. Figure 4.4 shows the model vs. data results for PHEN.

4.5.4 Summary Of Wind Tunnel-Lysimeter PAH Emission Data

A complex series of chemodynamic processes control and influence the chemical release and the flux of semi-volatile PAHs to air from the IHC DM. Solids consolidation and water expressed from the bed are major factors. The presence of ponded water provided a diffusion barrier on the surface keeping the fluxes low at the start of the volatilization process. During drying as un-saturated soil is produced, air-filled pore spaces encourage increased volatilization rates. This occurs because as noted previously chemical diffusivities

in air are more than 5000 times larger than those in water. The gradual drying process delays the onset of the maximum observed flux. During this period, dry soil patches appear on the surface and grow in number as time progresses. The maximum fluxes were manifest after 7 to 20 days depending on the initial DM water content. Beyond these maximums, the observed chemical fluxes decrease with increasing time. The rate of decrease was non-linear with increasing time and measured fluxes remained relatively elevated for upwards to 40 days. Additional discussions concerning the flux vs. time behavior patterns appear in the theoretical analysis section.

4.6 Model Development

The soil-to-air chemical volatilization modeling is based on observations made within a L/WT designed and operated using conditions similar to those found in the outside environment. Each of the experimental runs displayed chemical flux events classified into three water regimes. A conceptual graphical description of the three regimes is shown in Figure 4.5 in order to clearly identify the key aspects of each in the combined water-chemical evaporation-emission process.

4.6.1 Regime-0

After the dredged material was transferred from the drums into the lysimeter, it was nearly completely submerged under a layer of water. Only two chemical phases, liquid and solid, exists during this regime leaving the bed pore spaces between the solid particles saturated with water. The depth of this water layer was controlled by the topological variations of the DM surface. Regime-0 ends at time t_b when the water layer is effectively absent from the DM surface. Emissions of the contaminants during this time occurred by the chemicals diffusing from the water to the bulk air above. Fluxes from this regime were

generally very low. Volatile emissions for the ponded scenario are not within the scope of this study. However, the ponded scenario is important for hydraulic dredge generated DM and it will be addressed in a subsequent report. Regime-0 is therefore not modeled and is further considered only to the extent it initiates Regime-I.

4.6.2 Regime-I

At the end of Regime – 0 free standing water is absent; a wet DM remains. As the water consolidation-evaporation process continues Regime–I commences with dry patches being formed on the surface of the DM. These continue to be formed and completely cover the surface at time, t_D. Throughout this period, the air-filled pore-space patch areas increase from 0% to 100% as shown in Figure 4.6.

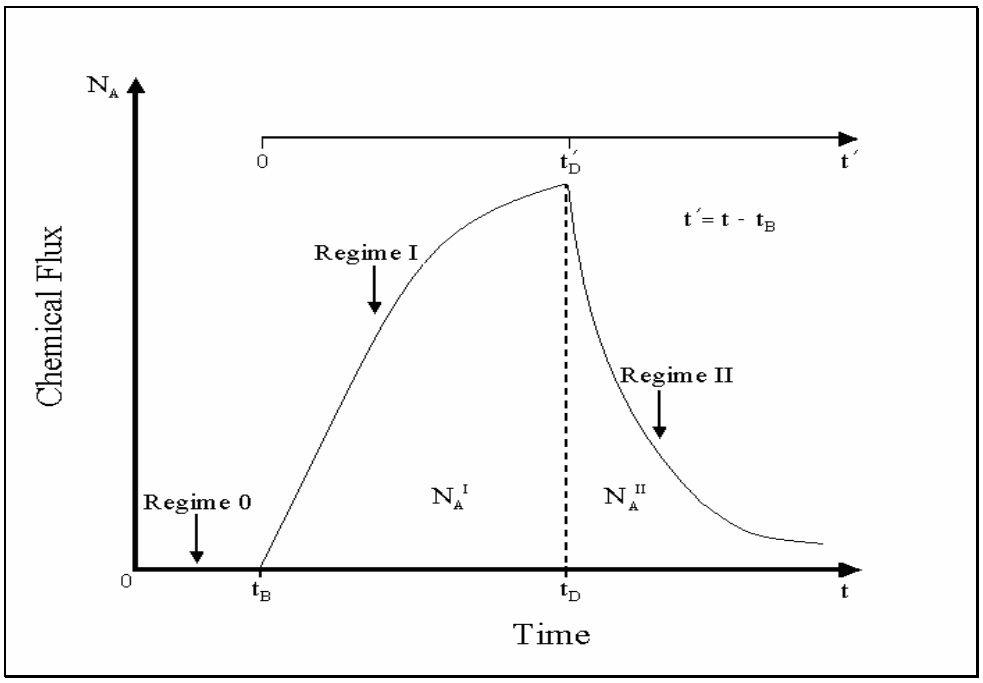

Figure 4.5 Exposed Dredge Sediment Regimes

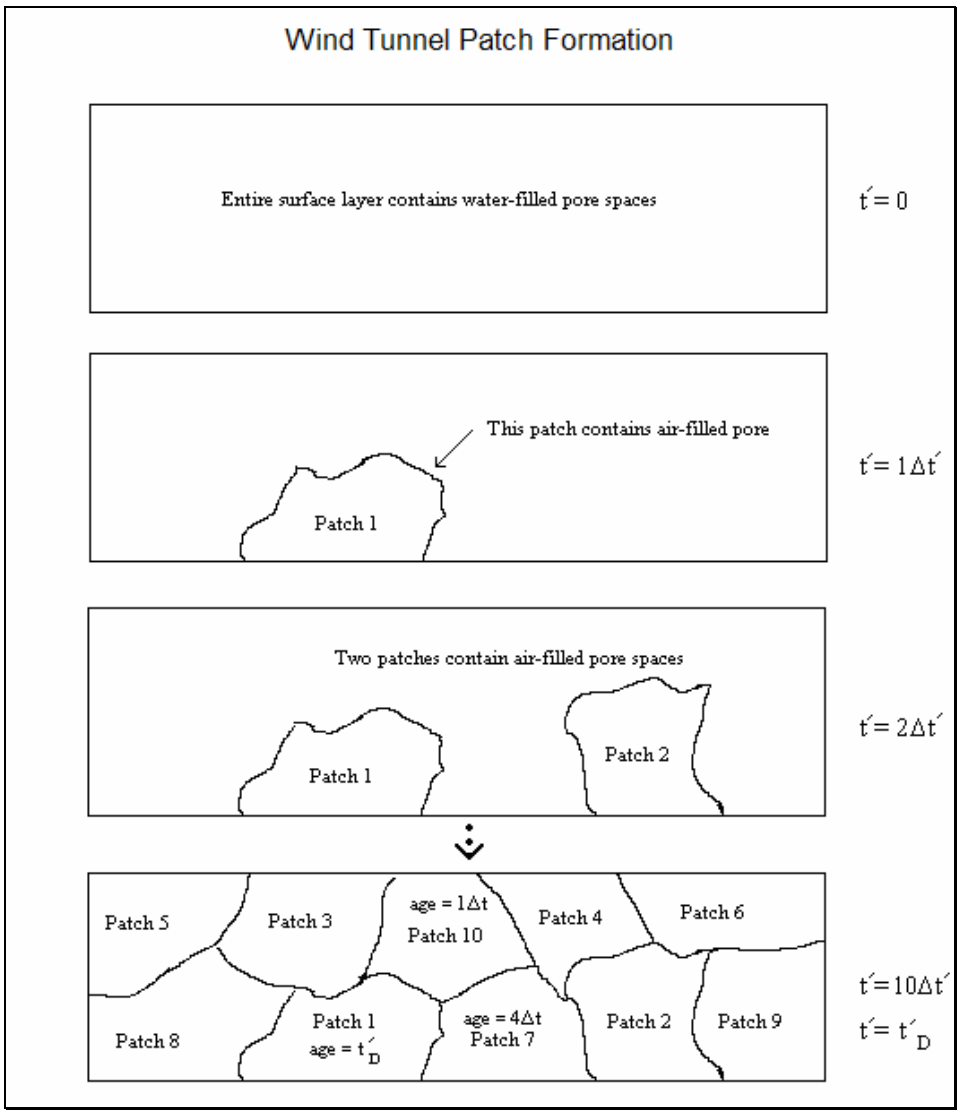

Figure 4.6 Linear Patch Age Distributions on DM Surface

These patch areas appear as the water-filled pore spaces are converted to gas-filled ones. The surface drying time, is $t'_d = t_d - t_{b,}$ the time period at the end of Regime-0 until the time the entire surface layer is covered with dry patches. It is an empirical parameter controlled by the combined consolidation and evaporation processes that drives liquid from the surface layer. The above equation defines the relationship between the run time t and the model time t′.

At the end of Regime – 1 a linear decreasing age distribution of equal size dry patches is assumed to exist. Figure 4.6 illustrates the size and age distribution for a hypothetical 10-patch surface. The first patch formed has an age of t'_d. After time interval Δt, the second patch was formed; its age at time t'_D will be $t'_D - \Delta t$. Rather than 10 patches the drying time period t'_D may be divided so as to produce n patches. For example, if one hour is a convenient value for the time interval Δt then the number of patches in the model is $n = t'_D / \Delta t$. For n time periods, the last patch formed has age equal $t'_D - (n-1)\Delta t$.

4.6.3 Regime-II

Regime-II commences after the last dry patch is formed. At the beginning of this regime air-filled pores are present throughout the entire surface of the DM bed. The chemical contaminant desorbs from the damp solid phase and diffuses through the porous, air-filled soil layers and into the bulk air above. The maximum chemical flux results at time t'_D. The evaporation/consolidation process continues, but at a slower rate. As it does, further pore openings widen in the present air-filled pore spaces and more are created at depth. Surface cracks form and widen as well. Chemical movement from the DM surface layer causes depletion. Deeper residing chemical quantities have a longer and more torturous diffusion path to traverse to get to the interface and this lowers the flux. This chemical depletion process was demonstrated in the laboratory for porous soils (Valsaraj, et al., 1999). The flux continues to decrease with increasing time. The next section contains a mathematical model developed to quantify these described flux behavior patterns.

4.6.4 Flux Equation

The basic flux equation used in this study has been shown to provide reasonable estimates of chemical volatilization from natural and agricultural soils to air (Thibodeaux, L.

J., et al. 2002). A Lavoisier's species mass balance was used in developing the equation for the case of a soil column of infinite depth containing an air interface at the top. A total of three phases (soil, air, and water) are assumed to be present. The model also assumes a uniform chemical loading concentration, C_S, throughout the soil column. The following algorithm describes the instantaneous flux for a chemical species through the air-filled pore-spaces, then through the air boundary layer and finally entering the bulk air above:

$$N = \frac{C_f \cdot \left(\frac{C_s \cdot H}{K_d} - C_{ai} \right)}{\sqrt{\frac{\pi \cdot t'}{D_{a3} \cdot \left(\varepsilon_1 + \frac{K_d \cdot \rho_b}{H} \right)}} + \frac{1}{K_G}} \qquad (4.2)$$

The above equation was incorporated in modeling algorithms developed for Regimes I and II. A model simulation using beds of finite thickness and infinite thickness indicates that identical fluxes are achieved for bed thicknesses of 3 cm or greater. Laboratory experiments with three PAHs for 35 days of evaporation showed chemical losses occurred only in the top 2cm of the sediment (Valsaraj, et al., 1999.) As illustrated in Figure 4.5, the chemical flux to air from the surface of the DM consists of two-regimes. The two-regime conceptual structure described previously forms the basis upon which to formulate the chemical emission process model.

4.6.5 Chemical Flux In Regime-I

The time-period t'_D (hr) will be divided into a number, n, of equal time-intervals Δt as noted above. Each time interval will have an average flux dependent on the age of the patch. The number of dry patches is also n and their rate of appearance (i.e., n/t'_D) will be assumed to be constant with time. For the first time interval (i=1) one patch exists; its area is $A_1/A = \Delta t/t'_D$; where A is the total surface area of the DM emission source and A_1 is the surface area

of a dry patch. The patch flux is computed as the average of that at t′=0 and t′=1Δt by applying Equation 4.2: this flux is denoted by N(1). This newly formed patch has the highest flux since t′ is small. The average flux for the entire emission source is denoted by $N_A(1)=N(1)\cdot A_1/A$. For the second time interval, i=2, patch 1 has increased in age; its flux is the average of that at t′=1Δt and t′=2Δt; it is termed N(2). It has a slightly smaller flux now since it has aged. Equation 4.2 accounts for the decrease in flux at its new age. The flux of Patch 2 is N(1) which was the previous value for Patch 1. The average flux for the emission source consisting of two patches is: $N_A(2)=[N(1)+N(2)]\cdot A_1/A$. In general for the i^{th} patches the emission source flux is:

$$N_A(i) = \frac{A_1}{A}\cdot \sum_{k=1}^{i} N(k) = \frac{\Delta t}{t'_D}\cdot \sum_{k=1}^{i} N(k) \qquad (4.3)$$

The ratio A_1/A is a constant and t′=iΔt. This equation relates the flux for each time interval $t'= t'_D$. As total patch size increases so does $N_A(i)$. The general shape of the function reflecting the increasing fluxes of Regime-I as expressed by Equation 4.3 is $N_A(t')$ vs. t′. For numerical computation of the flux using Equation 4.3, a time interval, Δt, for patch formation must be selected. Realistic values are one-half to one hour. Large time intervals such as eight hours will not realistically capture the time varying flux early in the patch formation process. Time intervals of minutes or less increases the number of patches and the number of intervals but may not necessarily increase computational accuracy. Numerical computations performed have shown that the N(i) function remains unchanged in magnitude as Δt takes on values less than 1 hour. At time t'_D, the flux $N(t'_D)$ is at its maximum value. Up until that

time, new patches were being formed. As time progresses beyond t'_D, Regime-II commences and no new patches are formed.

4.6.6 Chemical Flux In Regime-II

At the start of Regime-II, the surface of the emission source is covered with a mosaic of j patches of equal size and a linear decreasing age distribution ranging from Δt to t'_D. The oldest patch has age t_D' and the youngest has age Δt. As time progresses, all the patches become older. For example, the emission source flux for the sum of all n patches at $t'=t'_D+\Delta t$ is:

$$N_A\left(t'_D + \Delta t\right) = \frac{A_1}{A}\cdot\left(N(\Delta t) + N(\Delta t) + ... + N\left(t'_D + \Delta t\right)\right) \tag{4.4}$$

Where N is the average of the individual patch fluxes across each age interval. Each patch is Δt older. The oldest patch has age $t'_D+\Delta t$. Since the number of patches remains constant at n and as time progresses their individual fluxes decrease, the sum decrease as well. In general the emission source area flux for the time $t'=t'_D+j\Delta t$ starting with j=1can be expressed as:

$$N_A^{\Pi}(t') = \frac{A_1}{A}\cdot\sum_{k=0}^{n-1} N\left[(k + j)\cdot\Delta t\right] \tag{4.5}$$

The functional behavior of this equation is illustrated in Figure 4.5. As with Eqn. 4.4 the individual patch average fluxes, N, are computed from Equation 4.2. As j increases so do t' and the N_A function of Eqn. 4.5. It displays a decreasing flux with increasing time since the flux from individual patches decreases with increasing age (i.e., t' becomes large in Eqn. 4.2). Figure 4.5 shows the patch times corresponding to the fluxes N_A^I and N_A^{II}.

4.6.7 Model Applications To Wind Tunnel Data

The structure of the emission model and the associated flux algorithms were presented above. A two-regime emission structure defined by t'_D, the surface drying time, along with Equations 4.3 and 4.5 constitute the quantitative process model. Equation 4.2 is embedded and used to compute the chemical fluxes needed at the appropriate times and patch ages. The model was fitted to the measured fluxes obtained in Runs 1, 2, and 4. The model calculated and the measured fluxes appear in Figures 4.2, 4.3, 4.4 for NAPH, M-NAPH and PHEN, respectively.

Several transport, thermodynamic, and soil parameters are needed for Equation 4.2. These include the chemical molecular diffusivities in air, Henry's constants and the soil-to-water partition coefficients. These numerical values used appear in Table 4.2 in addition to the chemical loading and the air-filled soil porosities. Direct measurements were available for the IHC DM for all the parameters except the diffusivities. These were estimated based on the Fuller, Schettler and Gidding's algorithm (Fuller, et al. 1966). The following procedure was used in fitting the two-regime soil-drying model to the flux measurements.

Table 4.2 Transport and Thermodynamic Parameters of IHC DM at 25C

Parameter	Units	NAPH	M-NAPH	PHENAN
Molecular diffusivities, D_{a3}	cm^2/h	252.8	234.1	215.1
Molecular weight	g/mol	128	156	178
Henry's Constant, H_s	-	0.0198	0.0178	0.0021
Solid-to-Water Partition Coefficient, K_d	L/kg	260	1440	7017

+Analysis detection limit minimum

The calibration process commenced with a visual inspection of the graphical representations of the measured fluxes vs. runtime for each chemical. These appear in Figures 4.2, 4.3 and 4.4. First the ponded flux time-period, t_b, of Regime-0 was estimated for each run and the time positions, t, readjusted by subtracting t_b from the run time so that Regime-I begins at the origin (i.e., $t'=0$). These adjustments are reflected in the data points

re-plotted with the new times as shown in Figure 4.2, 4.3 and 4.4. The t_b's appear in Table 4.1.

Again, based on a visual inspection, the drying time, $t'_{D,}$ was determined. The conceptual schematic shown in Figure 4.5 is used as a guide; based on the data in Figures 4.2 and 4.3 for each run the t'_D values are chosen. It is somewhat a "judgment call" to establish at what time the maximum flux occurs faced with sparse data sets such as those appearing in Figures 4.2 and 4.3. This t'_D is a key adjustable parameter in the two-regime drying model. Nevertheless, reasonable values can be obtained and these appear in Table 4.2 for each run; the same values were used for each chemical.

In order for the model to mimic the measured flux vs. time data for each chemical unique values of K_G, the air-side MTC were needed. This is a the parameter which controls the rate of the flux rise with increasing time, its maximum value and it also influences its rate of flux decrease for times beyond time t'_D. The numerical values of K_G appear in Table 4.2. A "flux calibration factor", C_f, was needed to scale the absolute magnitude of the model-computed fluxes. Positive C_f values were needed to adjust the computed fluxes to the measured ones. These C_f values appear in Table 4.2. Figures 4.2, 4.3 and 4.4 contain the Regime-I and II measured fluxes and the model predicted fluxes based on the above calibration procedure for NAPH, M-NAPH, and PHEN respectively.

4.7 Discussion Of Results

The traditional approach to the subject of drying beds of solids employs the concept of the constant-rate period and the falling rate period (Perry, 1950). Moisture (i.e. water) is the "drying" chemical of primary focus in this traditional field where uniform granular solids particles typically constitute the beds. Water is present in DM in copious amounts and likely

undergoes both a constant rate and a falling rate-drying period. The data shown in Figures 4.2, 4.3 and 4.4 clearly demonstrate that this traditional approach does not apply to NAPH, M-NAPH and PHEN evaporation (i.e., drying) since there is no constant rate period. Nevertheless, the presence and behavior of water in the DM is a significant process factor. The published literature on traditional, non-consolidating solids drying by water evaporation is voluminous. Because the combined processes of water consolidation, ponding, run-off, and evaporation are exceedingly complex in the case of DM drying an empirical approach containing some theoretical aspects of the traditional drying process was adopted. This approach was used for Regime-I as was developed previously. The essence of the approach is the idea that "dry surface" patch areas of air-filled soil pore-spaces is assumed to appear linear with time and to occupy the entire emission surface at time t'_D. A linear function is consistent with the concept of moisture evaporating from the surface of the bed at a constant rate. Once the surface becomes dry the water evaporation rate falls. It is assumed that the constant water evaporation rate period ends at the drying time, t'_D. A chemical flux to air process was superimposed onto the constant rate period and is consistent with the dry patch formation process. This interpretation allowed the development of a simple computation procedure for the chemical emission flux behavior during Regime-I. The ability of the model to mimic the observed increasing chemical fluxes (i.e. zero to maximum) is apparent in Figures 4.2 and 4.3.

Since the water behavior controls t'_D it should be chemically independent, theoretically. This appears to be so for the NAPH, M-NAPH and PHEN flux data; the t'_D values appear in Table 4.2. However, t'_D, the drying time, is different for each experiment. Rewetting the DM solids to its original water content after Run 1 was unsuccessful. Only a

fraction of the original water was reintroduced and as a consequence, the drying times for Runs 2 and 4 were shorter. The t'_D values of 125 hours and 100 were needed for Runs 2 and 4 compared to 425 hours for Run 1. Nevertheless, based on this limited data set it appears that the semi-theoretical dry patches model is consistent with traditional solids-water drying concepts.

The highest chemical fluxes occur from the individual patches when they are first formed. Setting t=0 in Eqn. 4.2 yields the highest flux which occurs when the airside MTC, K_G, controls the process. High fluxes are seen as each new patch is formed. The numerical value of K_G therefore plays a dominant role in the magnitude and shape of the rising fluxes characteristic of Regime I. The chemical flux from a patch quickly diminishes as time increases, according to the $t^{-1/2}$ relationship in Equation 4.2. Therefore, the numerical value of K_G is an important adjustable parameter in Equation 4.2 for mimicking the flux behavior in Regime I. The K_G values of NAPH, M-NAPH and PHEN appear in Table 4.3 and are based on a visual fitting of the model fluxes to the data.

Table 4.3 Emission Model Calibration Parameters

Parameter	Units	NAPH	M-NAPH	PHENAN
t_b, ponded flux time interval; (Run 1/ 2/ 4)	hours	3/ 2/ 5	3/ 2/ 5	3/ 2/ 5
t_D, drying time; (Run 1/ 2/ 4)	hours	425/ 125/ 100	425/ 125/ 100	425/ 125/ 100
K_G, air-side mass transfer coefficient	Cm/h	672	640	604
C_f, flux calibration factor; (Run 1/ 2/ 4)	-	17/ 4/ 10	50/ 15/ 27	12/ 4/ 7

Theoretically for a constant wind speed, the effective K_G in the wind tunnel should be constant and therefore independent of experimental run. This is the case, apparently, because the wind speed was kept constant for all three runs and same numerical values of K_G resulted. The K_G values are chemical dependent and a function of its molecular diffusivity in air D. The calibrated K_G values were correlated with D^n where $n \cong O.64$. This result is consistent with boundary layer theory where $K_G \cong D^{0.67}$. In addition numerical values of K_G's for

organic chemicals similar in size have been reported in the range 100 to 1000 cm/h and depend on windspeed (Thibodeaux, L. J., et al. 1985). Therefore the 600 to 700 cm/h range for the effective K_G's observed in the L/WT tunnel are very consistent with this range of values.

The two adjustable parameters needed for this two-regime emission model, t'_D and K_G, have a good theoretical basis and are well constrained as to their numerical magnitudes. They cannot be arbitrarily adjusted in order to force model vs. data congruence. A flux calibration factor, C_f, was created as a multiplier to Equation 4.2 because its use with appropriate t'_D and K_G values consistently underestimated measured fluxes. Nine values of C_f were needed; these appear in Table 4.3 and range from a +5 to +50. The C_f's for M-NAPH are larger than those for NAPH; the averages being 31 and 10, respectively. PHEN displayed the lowest C_f values with an average of 8. Such model vs. data flux deviations have been observed in laboratory experiments with soils, which behave very unlike DM (Thibodeaux, L. J., et al., 2002). However, in the case of soils the model predications were typically higher, numerically, than the measurements. Soils typically do not undergo the particle consolidation process like DM. At this time the causes of the direction and magnitudes of C_f are unknown. The following provides a plausible reason for the C_f magnitudes being larger than unity.

Bed consolidation with water expressed in the upward direction followed by evaporation may have contributed in a significant way to the measured fluxes being larger than the model predictions. A single batch of DM was used in the three separate experiments. The mud level decreased 5.1 cm (2 in) at the end of Run 1. Each inch is equivalent to 140 L of H_2O. Thirty liters of water was added and the bed surface re-mixed

prior to performing Run 2. Compared to those measured in Run 1, the maximum fluxes of both chemicals were lower in Run 2 by a factor of three. 520 L of water was added after run 2 and the bed remixed prior to Run 4. The maximum fluxes returned to the levels of those observed in Run 1. It appears that when massive quantities of water were being mobilized from the bed, as happened in Runs 1 and 4, high chemical fluxes were observed. Much lower fluxes occurred in Run 2; where little water was present to mobilize through the combined consolidation/evaporation process. No water was lost downward or collected as leachate. The upward moving water may be transporting fine particles to the surface of the bed at which time they are deposited.

The solids-water mixing and homogenization process that occurred in the lysimeter prior to each run may have contributed to the placement of a thin soil layer containing elevated chemical concentrations on the DM surface. The solids-mixing process produces a supernate rich in fine particles since the sand and silt fractions settle rapidly. In effect this combined mixing-settling event is a crude fractionation process that produces a "raffinate" phase consisting primarily of large particles and some water. This phase is overlaid by a "supernate" phase consisting of fine particles in suspension. As the water evaporates in Regime – 0 these fines are deposited on the surface. These fines, which include the clays and organic colloids, typically contain higher chemical loadings (i.e., C_S in mg/kg) per unit mass than the average. Pilot-scale and laboratory derived evidence was found that supports the surface layer enrichment process.

A pilot-scale demonstration of Saginaw River, MI sediment washing treatment was performed using individual equipment modules roughly the size of the L/WT apparatus (EPA, 1994). DM daily feed quantities of 8 to 20 m^3 were "washed" through a series of

devices consisting of hydrocyclone separators, dense media separators, attrition scrubbers, sand recovery and dewatering screens and final clarifiers. Eight-grain particle size classes were used to assess the effectiveness of the washing. The largest was 430μm sand and the smallest was 30μm fines. Since contaminant concentration/volume reduction is simply an artifact of the partitioning for the contaminants among these grain sizes an extensive effort was made to monitor these as they moved through the soil washing system. Approximately 19% of the feed was in the < 30μm range. The total organic carbon (TOC) enrichment factor (i.e., concentration in discharge stream to the feed concentration) was nearly 20 for the particulate organic fraction (size > 109μm). Polychlorinated biphenyls (PCBs) with mean a feed concentration of 1.2 mg/Kg as total Arochlors, displayed a mean enrichment factor of 3.8 with a maximum of 9.4 in the clarifier solids. Separate laboratory, bench-scale test, enrichment factors of 6.2 were observed for the PCBs in the Saginaw sediments. In another laboratory study, PAHs in NJ/NY Harbor sediments were separated into size fractions and further separated into low and high density fractions in an effort to better understand the factors controlling sequestrations and desorption in the field (Rockne, et al., 2002). The PAH concentrations were found to be greatly increased in the low-density fraction and not predictable by equilibrium partitioning theory. For the Piles Creek (PC) sediment the low density-to-bulk concentration total PAH ratio was 19 while that for Newton Creek (NC) was 3.2. In addition it was found that the PAH partition coefficients (i.e., K_{oc}) were nearly 10 times larger for the low-density fraction.

The above studies illustrate that elevated chemical concentrations appear in the fines and/or low-density particle fractions. Generally the enrichment factors ranged from 3 to 20. The evaporation of a standing water layer above a DM solid bed will deposit fines particles

with elevated chemical concentrations on the bed surface. Chemical volatilization may be driven by the enriched interface concentration producing higher fluxes than represented by the average concentration in the DM. Run 2 had too little water moving upward so the surface received little or no concentration enhancement; therefore the maximum fluxes for NAPH and M-NAPH were 3 times lower compared to Runs 1 and 4. Since the average concentration was used in the model rate equation to compute the fluxes, the predicted results should be lower and they were. The flux calibration factors for Run 2 were correspondingly lower than those required for Runs 1 and 4. It appears that the upward particle-bound chemical mobilization process that results from bed consolidation and evaporation may contribute to the high measured fluxes. The chemical emission algorithm, Equation 4.2, employed in the predictive model originates from theories and laboratory testing of chemical transport in surface soils that do not consolidate and therefore water is not expressed upward. Although this is a logical explanation for the model vs. data mismatch, and the need for the C_f corrections there may be other factors or processes involved.

4.7.1 Model Field Application

Freshly applied DM from mechanical dredging will likely behave differently from that used in the L/WT. If the DM retains the low in-situ water content of the sediment bed when deposited upon the CDF surface only limited consolidation will occur. The small quantities of expressed water will run-off to a designated ponded basin prepared for its collection. Evaporation of water from the surface of the exposed DM solids will commence immediately and dry surface patches will likely appear fairly rapidly. In the L/WT the DM was homogenized and water mixed in to produce uniform chemical concentrations, which was necessary for making consistent measurements needed for flux model comparison. The

L/WT was not designed for runoff applications so water had to move upward then evaporate to depart the DM mass. This kept the DM surface supplied with moisture and prevented it from drying quickly. Two model parameters, t'_D and C_f, must be addressed in translating the L/WT results to the field.

Drying times were very long, these being 4 to 18 days. In this regard the L/WT experiments did not simulate the field drying solids conditions. Drying times in the field will depend primarily upon the local wind speed, temperature and the air relative humidity. Except for extended rain periods the field drying times will be rapid and are better represented by the low-end of the L/WT values. Times much less than 4 days and in the 8 to 24 hour range may be reasonable under excellent soil drying conditions. The value selected for t'_D is left to the judgment of the user. The tipping and spreading of DM "lifts" deposited from trucks, for example, produces a complex geometric footprint surface containing a range of drying times. In reality t'_D for a particular tip may not be attainable. A default value of 24 hours takes into account the dominance of the solar factor in drying.

Without the occurrence of Regime-0 the use of a model flux enhancement factors, C_f greater than unity are not necessary. In the field rapid water runoff will allow little opportunity for a continuous layer to develop on the DM surface. Without its presence and subsequent evaporation no surface deposit with enhanced chemical concentrations can be formed. For a CDF receiving solid dredged material such as typically derived from mechanical dredging operations a $C_f = 1$ is recommended.

Normally during hydraulic dredging the CDF contains ponded water and appropriate models are available for estimating these emissions. However, exposed surfaces containing solids do occur during the life cycle of a ponded CDF. Deltas are formed in the vicinity of

the pipeline slurry entering the CDF. Also a drying solids bed is formed during the latter days of filling when the ponded water is drained away prior to closure. The use of the drying solids emission model is appropriate in both these cases.

The two primary parameters mentioned as being key parameters are t_D and C_f. In applying this model to a dredging site, weathered conditions must be accounted for when calculating the emissions from exposed dredge material that has already consolidated. The results from the experimental runs showed that any attempt to incorporate water back into the sediment is a failure. This can correlate well with rain and weathering to the sediment. Once the sediment undergoes the initial consolidation, the sediment cannot regain the pore space volume. This is useful for designating a dry time for weathered sediment. The Runs 2 and 4 show the same t_D even after trying the incorporate water back into the bulk sediment. This allows the model to contain some percentage of the initial t_D for $t_{Dweathered}$. As shown from experimental results, the t_D post Run 1, $t_{Dweathered}$, are consistent at ~25% of t_D. The correction factor did however become affected in Run 4 compared to Run 2 by the addition of water. This demonstrates that the weathering will impact the correction factor. This $C_{fweathered}$ is some fraction up to 100% of C_f. These topics discussed above are to provide the user with some type of approach to dealing with modeling long time emissions.

Further guidance in applying the model to the field appears in the report entitled: "Volatilization rates from dredged materials and soils – A literature review" (Thibodeaux, et al., 2002).

CHAPTER 5

PONDED CDF EMISSION MODEL

5.1 Model Overview

In the case of hydraulic dredging, the dredge facility consisting of the extraction machine and the DM slurry operation is intimately connected to the CDF. These connections are illustrated in Figure 5.1. At the dredge, the dredge material is extracted with partial solids and the balance of water combined to form Q_{ds}, which is the calculated flow of solids and water from the DOU. The DM is mixed with water to create as solid-to-water ratio slurry that can be easily pumped to the CDF through a pipeline. From experience such ratios are well established. Make-up water, Q_M, from the stream or embayment may be used to create the appropriate ratios. However, this stream eventually emerges from the discharge of the CDF and must be treated prior to entering the waterway. Since water treatment is costly during steady-state operations the CDF discharge can be wholly eliminated by using recycle water as shown in Figure 5.1. Only during dewatering the CDF at the end of the dredging season is water discharge treatment required.

During dredging from the DOU, the slurry exit stream flows into the CDF entrance. Within the CDF, suspended solids are removed from the water column by settling to the bottom. Sand separates first followed by the silt size particles and finally the clay fraction settlers. A shallow sloping sediment-water surface develops along the length of the CDF from the entrance to discharge. This process is illustrated in Figure 5.2. As shown below, a water column exists within the CDF. The surface in contact with the air is the source of the volatile chemical emissions.

Weirs or other level control devices maintain a fixed water elevation. As time

progresses during the dredging season, solid material slowly replaces the water mass and the average water column depth decreases. Upon reaching its design capacity the remaining water column is drained. After draining, the DM is allowed to consolidate and stabilize before final closure.

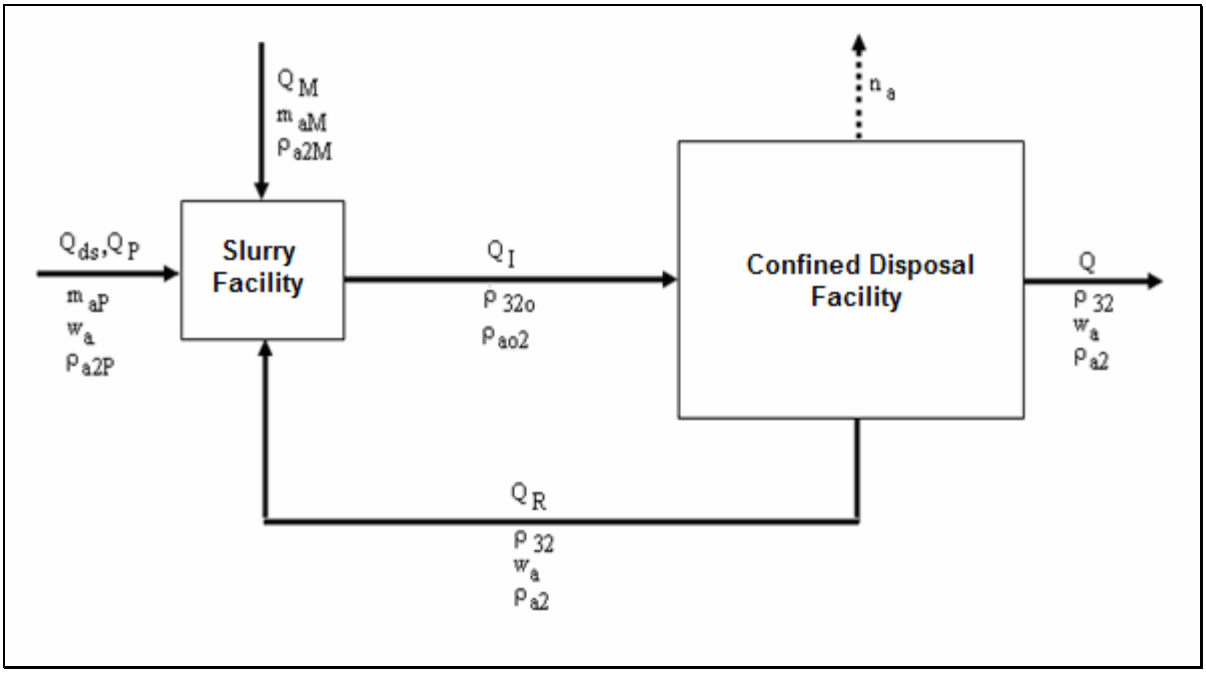

Figure 5.1 Conceptual Illustration Dredge and CDF Operations

From a daily operation perspective and for the seasonal one as well, many aspects of the CDF operation are transient. Concentrations of chemical and suspended solids are constant changing with position within the unit as well. Most of these fluctuations are unknowable and therefore unpredictable. The approach in the modeling effort will be to assume a steady state operation and to accommodate variable changes that capture the most conservative emission predications. For example, the hydraulic flow model for the water through the CDF will be assumed to be plug flow. This maximizes the chemical concentrations in the water column, which in turn maximizes the emissions to air. Since the water depth column is known to change slowly over time. At least two depths, one deep and

another shallow, operated at steady state will bracket the hydraulic retention times that are known to affect the emission rates.

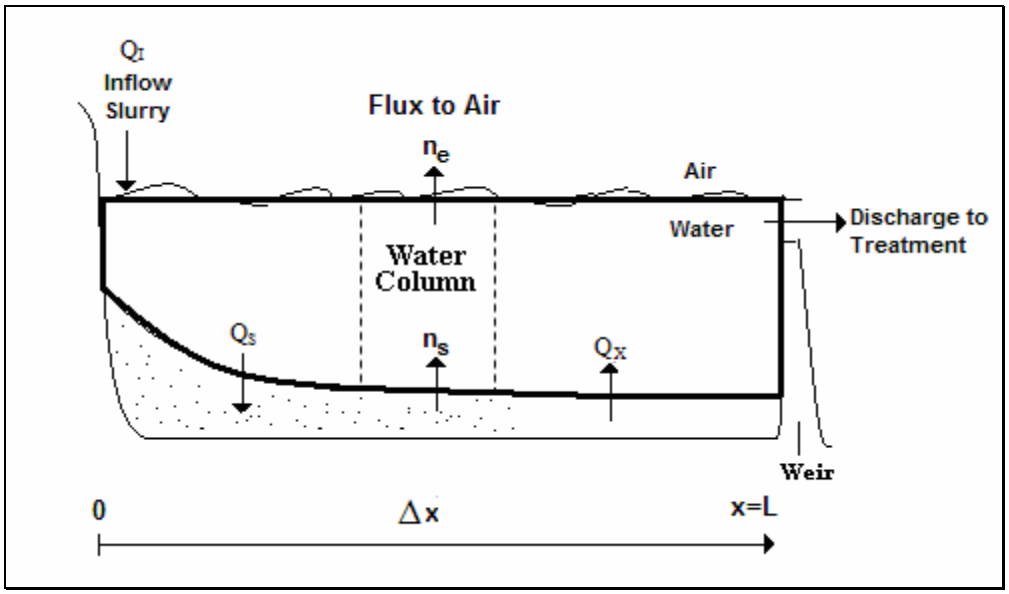

Figure 5.2 Ponded CDF Profile View

The following section contains the details of the model for emissions from a ponded CDF. In the development, additional assumptions will be needed. In all cases, they have been chosen so as to maximize the model predicted fluxes. The model consists of three simultaneous mass balances; solids, water, and chemical. Once single final algorithm is produced that represents the chemical flux for a CDF operating with water recycle. However, it can be used for the so-called conventional CDF operation that has once-through or one-pass water use. This case is simulated by setting the recycle stream flow rate to zero.

5.1.1 Solids Balance

The dredge extracts material, solids and water, from the bed at a constant volumetric rate of Q_{ds} (m^3/s). This volumetric flow consists of a fraction of pore water that can be defined by Q_P (m^3/s). The remainder is dry solids of rate m_P (kg/s). In order to meet the

slurry pumping requirements of solids in water concentration of ρ_{32o} (kg/m^3), the solids mass balance around the balance around the dredge facility shown in Figure 5.1 is:

$$m_P + m_M + m_R = Q_I \rho_{32o} \tag{5.1}$$

where Q_I is the volumetric water rate entering the CDF (m^3/s) and the recycle water Q_R (m^3/s). This result can be solved for Q_I since the solids in the make-up and recycle water is insignificant in comparison to the dredged solids. A typical value for ρ_{32o} is 170 kg/m^3.

5.1.2 Water Balance

For the dredge facility, the steady state water volumetric balance is:

$$Q_P + Q_M + Q_R = Q_I \tag{5.2}$$

where if there is no recycle used $Q_R = 0$. As shown in Figure 5.1, the recycle stream connects the dredged facility with the CDF. The water flow from the DOU can be evaluated as follows:

$$Q_P = Q_{ds} \varepsilon_2 \tag{5.3}$$

where ε_2 is the water volume fraction. The Q_{ds} can be determined for a mechanical dredge by an estimated volume of sediment excavated and cycle time of dredge arm. Other water flows include precipitation inputs as rain or snow and outputs such as evaporation. It is assumed that these are approximately equal so they balance each other and don't appear in the figure.

The CDF water balance is slightly more complex. Some internal flows are important; see Figure 5.2. As the slurry enters the CDF, the solid particles quickly settle forming a mud layer on bottom consisting of high solids to water ratio or initial bed water porosity ε_I. This results in the temporary capture of much water at a rate of Q_S (m^3/s) between the settling solids. This flow is considered an outlet flow since the volume under evaluation is considered the changing newly deposited solid surface. As time proceeds, bed consolidation

occurs where the particles pack together gravity acting on the solids and the water column force acting on the surface of the bed thus eliminating pore water. Final bed water porosity of ε_F results in as return flow of pore water upward occurs. This rate of expressed water flow to the water column from the bed contraction process is Q_X (m^3/s). The difference between is the called the "bulking losses" water rate Q_B which has a net downward flow. In effect, this portion of the slurry water remains in the CDF bottom sediment as pore water. The CDF water steady state balance is:

$$Q_I = Q_R + (Q_S - Q_X) \tag{5.5}$$

where

$$Q_B = Q_S - Q_X = \frac{Q_I \cdot \rho_{32o} \cdot \varepsilon_I \cdot \left[1 - \left(\varepsilon_I - \varepsilon_F\right)\right]}{\rho_b \cdot \left(1 - \varepsilon_I\right)} \tag{5.4}$$

and ρ_b is the bulk density (kg/m^3). The other terms have been previously defined.

The consequences of the bulking loss with the Q_S and Q_X flows become important to the chemical mass balance. They represent a chemical accumulation mass and advection exchanges across the sediment-water interface which impacts the effective water column chemical concentration and the volatile emission rate. These flows enter the chemical mass balance discussed next.

5.1.3 Chemical Balance

In Figure 5.2, the CDF includes a control volume element as a portion of the water column. It is of length (Δx), height or water depth (h), width (w), all in meters. Performing a steady state chemical balance on this CV allows for a desorption quantitative of the concentration in the water. The hydraulic flow is from left-to-right and the retention time is:

$$\tau = \frac{\Delta x h w}{Q_R} \tag{5.5}$$

The use of Q_R as Q even though Q_I is larger maximizes the model chemical residence time and the emission flux as well. Conceptually, the mass balance for volatile chemical A is:

$$Q_R\rho_a\big|_x + Q_X\rho_a{}^{**} + {}'K_{a2}[\rho_a{}^{**} - \rho_a]A = Q_R\rho_a\big|_{x+\Delta x} + Q_S\rho_a + {}''K_{a3}[\rho_a - \rho_a{}^{*}]A + \Delta x h w r_A \quad (5.6)$$

where the individual rates represent: advective inflow at position x, inflow of expressed pore water from the bed, diffusion-type mass transfer from bed surface, advective outflow, settling solids captured water outflow, evaporation to air and reaction degradation in the water column. Each term has units of kg-A/s. The concentration in the water column is ρ_a. The equilibrium chemical concentration that is expressed from pore water is $\rho_a{}^{**}$ and that in air is $\rho_a{}^{*}$. The ${}''K_{A3}$ is the sediment-water mass transfer coefficient (m/s) and ${}'K_{A2}$ the volatilization mass transfer coefficient (m/s).

Conceptually, Eqn 5.6 represents the chemical fate in the CDF. Convenient assumptions that maximize the flux are to assume no degradation/reaction ($r_A = 0$) and no chemical in the atmosphere $\rho_a{}^{**} = 0$. It is also assumed that chemical A is partitioned onto the suspended solids in the water column. Equilibrium partition between the solid and soluble phase is assumed here as well as in the pore water of the bed. With this included, Eqn. 5.5 is in the reality just slightly more complex in its derivation. The resulting differential equation is integrated from the inlet slurry flow concentration at x = 0 to the discharge position x = L where the water concentration is ρ_a at x = L. This result is:

$$\rho_{a2} = \rho_{ao2}\cdot\exp\left[\frac{-A_s\cdot\left({}''K_{a3} + {}'K_{a2} + v_s\right)}{Q_I\cdot\left(1 + \rho_{32}\cdot K'_{a32}\right)}\right] + \frac{\left({}''K_{a3}\cdot\rho'''_{a2} + {}'K_{a2}\cdot\rho'_{a2} + v_x\cdot\rho'''_{a2}\right)}{\left({}''K_{a3} + {}'K_{a2} + v_s\right)}\cdot\left[1 + \exp\left[\frac{-A_s\cdot\left({}''K_{a3} + {}'K_{a2} + v_s\right)}{Q_I\cdot\left(1 + \rho_{32}\cdot K'_{a32}\right)}\right]\right] \quad (5.7)$$

where the inlet concentration is:

$$\rho_{ao2} = \frac{\frac{\varepsilon_2 \cdot \rho_{32o}}{\rho_b \cdot (1-\varepsilon_2)} \cdot \frac{w_a}{K'_{a32}} + \frac{Q_R \cdot ("K_{a3} \cdot \rho'''_{a2} + 'K_{a2} \cdot \rho'_{a2} + v_x \cdot \rho'''_{a2})}{Q_{ds} \cdot [\rho_b \cdot (1-\varepsilon_2)] \cdot ("K_{a3} + 'K_{a2} + v_s)} \cdot \left[1 - \exp\left[\frac{-A_s \cdot ("K_{a3} + 'K_{a2} + v_s)}{Q_I \cdot (1 + \rho_{32} \cdot K'_{a32})}\right]\right]}{\left[1 - \frac{Q_R}{Q_{ds} \cdot [\rho_b \cdot (1-\varepsilon_2)]} \cdot \exp\left[\frac{-A_s \cdot ("K_{a3} + 'K_{a2} + v_s)}{Q_I \cdot (1 + \rho_{32} \cdot K'_{a32})}\right]\right]} \quad (5.8)$$

The chemical flux to air is obtained by the product of $'K_{A2}$ and ρ_a. Since ρ_a varies from inlet to CDF outlet, the flux must be summed at each point along the length (i.e. integrated) and multiplied by the CDF width to obtain the mass emission rate:

$$w = {}'K_{a2} lw[\overline{\rho_a} - \rho_a **] \quad (5.9)$$

where $\overline{\rho_a}$ is the average concentration, L is the CDF length and w its width. The emission rate, w, is in kg/s.

The next section contains a presentation of the relationships needed to obtain the various MTCs in Eqn. 5.7. As noted above, the solid associated chemical was included in the mass balance. However, a solids balance model as such was not performed. Field data based on observed TSS concentration were used instead as a substitute for the solids balance process model. The concentration of solid particles at the exit of the PCDF is assumed to be negligible because of the hydraulic retention time of the liquid generally being quite large which allows efficient particle settling (Personal conversation with Paul Schroeder, USACE, ERDC. Feb 2005). The focus on the exit waters deals with the chemical in solution for either treatment or for recycle.

5.1.4 MTC Correlations

With these process conditions within the PCDF, the chemical concentration in the water column can then be estimated for use in calculating the evaporative flux of chemical. The mass balance detailed above was used to determine the water column aqueous chemical concentration by developing the expressions for the flux terms and initial concentration. The

sediment flux acts as an input source for maintaining higher water column concentrations. In determining the sediment flux, the mass transport coefficient is estimated by the following expression.

$$K_{a32} = \frac{\frac{b \cdot C_D \cdot \rho_1}{\rho_2} \cdot v_1^2 \cdot h^{1.25}}{l \cdot M_a^{0.5}} \tag{5.4}$$

where b is the empirical constant 18.9 and the drag coefficient, C_D, is 0.00166. The velocity of wind (m/s), density of air (ρ_1, g/cm^3) and water (ρ_2, g/cm^3), height (m), length of PCDF (l, m), and molecular weight of the chemical (M_a) are used to estimate the mass transfer coefficient in units of m/s (Thibodeaux L. J. et al. 1982).

The individual MTC for the water/air interface is estimated using the local air-side and water-side mass transfer coefficients. The respective water-side and air-side MTCs are combined with the well known two-resistance theory. An existing correlation for ethyl ether is used for the liquid-side MTC. Graham's Law may be used to convert to other soluble chemicals.

$$'k_{a21ethylether} = 0.094 v_1^2 \tag{5.5}$$

An existing correlation for water evaporation from reservoirs is used to estimate the air-side MTC:

$$''k_{a12watervapor} = 358 \cdot v'_1 \cdot A_s^{-0.05} \tag{5.6}$$

The MTC is estimated in cm/hr for a known wind velocity, v_1 (m/s) or $v`_1$ (mph), and PCDF surface area, A_s.

5.1.5 Model Application

The focus of this section is to verify whether the model produces reasonable estimates using sample input parameters. The following section is not designed to provide actual results. These input values shown in Appendix B were estimated to evaluate the profile output of the model. The variables listed as the inputs along with the output figures were developed for modeling a ponded CDF with the inlet location fixed and a recycle loop modification. The results appear in Figure 5.5.

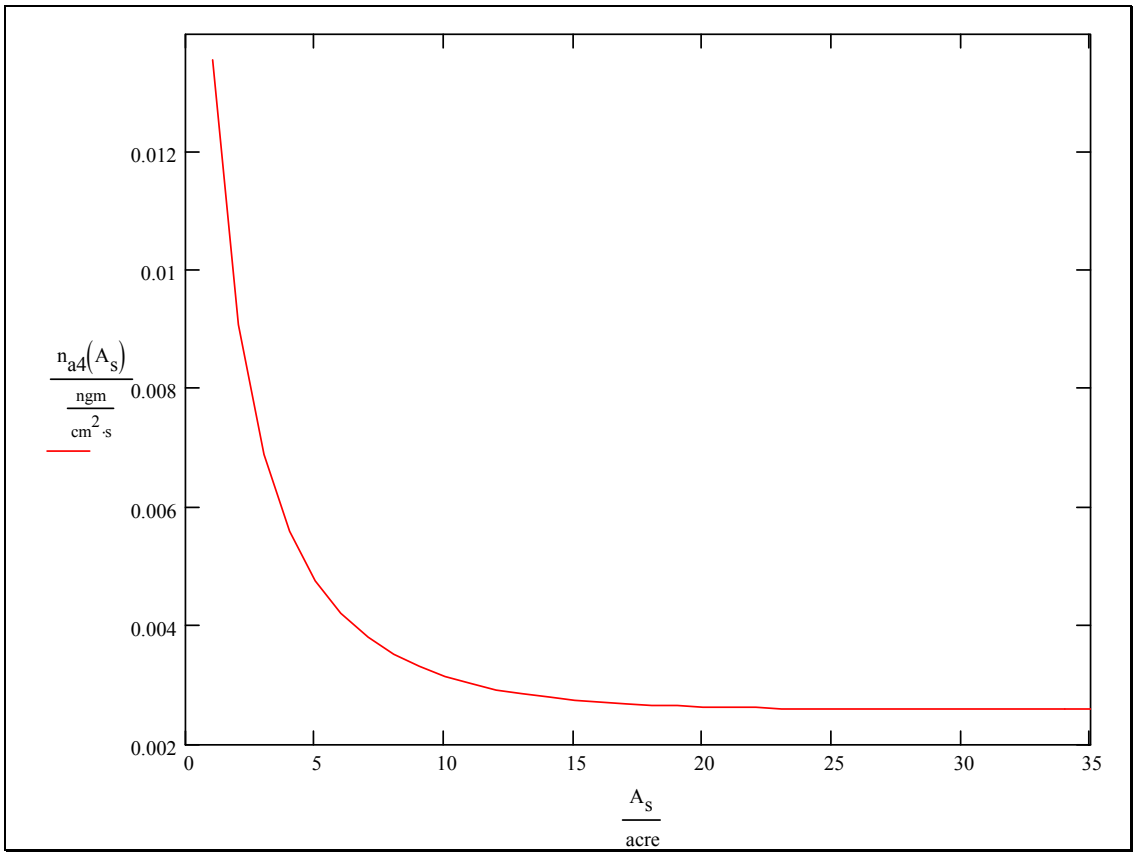

Figure 5.3 Chemical Emissions Profile for PCDF with Recycle

The results show the depletion of chemical in the water column over the length of the ponded CDF. At the beginning of the simulation estimates, the chemical concentration in the water column is driven by the incoming chemical in solution, suspended solids, and flux

from the bed sediment. After particle deposition process results in the water column becoming depleted of suspended solids, the driving force becomes the flux from the sediment bed. The slope of the concentration line decreases in the same manner as the sloping bed layer. This chemical concentration resulting primarily from the sediment chemical flux is the steady state CDF water chemical concentration, ρ_{A2SS}. The results will change as the parameters such as CDF area, dredge rate, and recycle flow change.

CHAPTER 6

MODEL CONCLUSIONS

The models provided in this document have been developed to aid in the planning of dredging operations by demonstrating methods used to determine chemical emissions to the air. In dredging, source of significant emissions can be found in two places; the dredge operable unit (DOU) and the confined disposal facility (CDF). In creating versatile models, these locales were expanded even further. The DOU model was broken down into three main scenarios. These include emissions from dredging enclosed rivers, rivers without enclosures, and embayments with enclosure. In each of these models, the chemical emissions consisted of an area producing a constant source of volatile emissions and another producing a plume of chemical either downstream in the case of the river or radial dispersion of chemical. In order to perform these calculations, these areas of chemical release were categorized into two zones. The forced convectional zone entails the area of the dredging operations that has mass transfer influenced by the disturbance in the water column and at the benthic layer by the dredge head. This zone is comprised of mass transfer coefficients for wind, hydraulic flow, and dredge disturbance. The natural convectional zone consists of the areas of the dredging which do not have enhancements due to the dredge disturbances in the water. Techniques were provided in order to estimate these mass transfer coefficients primarily for the dredge interaction with the chemical release. Methods for evaluating the area of the convective zones as well as the area of the DOU were provided for using the equations in calculating the chemical flux.

In the case of DM being exposed to air post draining the PCDF or transporting mechanically, a detailed model in Chapter 4 has been developed and verified using measured

data. The Army Corps of Engineers at WES developed a lab-scale wind tunnel with dimensions 16 ft in length, 4 ft in width, and 3 ft in height using a lysimeter as the base for the unit. DM from the IHC was transported to the lab to be used in measuring chemical fluxes. The model used was developed originally for modeling soils, but found to be useful in modeling sediment emissions by introducing the water changing patch formation concept. When chemical is released in soils, the chemical flux can be represented as a spike with a slow decay. This is primarily due to the soil containing air-filled pore spaces. These events changed for sediments after analyzing the measure results from the wind tunnel. The flux was found to steadily increase over time until reaching a point when it began to decrease rapidly. Through much understanding of the process of which the sediment incurred, a theory developed that the emissions from the surface were being released at a steady rate due to the drying undergoing in the surface layers. The idea of patch formation was developed to explain the drying of a surface in which chemical could then diffuse much faster through air instead of water. As patches formed, small burst-like spikes of chemicals occurred and then began to age. The aging process is critical in this understanding since it is essentially explains the slow steady rise of the chemical flux. After the dry patches cover the entire surface, the emissions are solely based on aging patches releasing less and less chemical as time passes. In developing this idea, the situation of exposed DM can be accurately defined with the models produced in Chapter 4 as long as the dry time can be estimated.

The disposal of DM can be performed by hydraulic transport in which the CDF fills with water to form a pond with solids in suspension. These solids are slowly being deposited over the length of the CDF depending on size. Large particles such as sand fall out close to the entry point as smaller particles float and deposit at some distance away from the entrance.

A sloping bottom sediment/mud layer forms in the CDF due to this deposition process. The emissions will closely match this type of profile as the model uses a plug-flow solution to determine maximum chemical emissions to the air. The model details the development of the chemical concentration in solution in the water column of the CDF. Modifications can be added to the conventional model to provide a recycle flow. The purpose of the recycle flow is primarily to decrease the amount of water requiring treatment. In adding the recycle term, the model compensates for the added aqueous chemical concentrating the incoming slurry.

REFERENCES

Assessment and Remediation of Contaminated Sediments (ARCS) Program REMEDIATION GUIDANCE DOCUMENT. *US Environmental Protection Agency. 1994. ARCS Remediation Guidance Document. EPA 905-B94-003. Chicago, Ill.: Great Lakes National Program Office.* http://www.epa.gov/glnpo/arcs/EPA-905-B94-003/B94-003.ch4.html

ASTM, 1998. Annual Book of ASTM Standards, West Conshohocken, PA. 1998. Copyright, American Society of Testing and Materials, 100 Barr Harbor Drive, West Conshohochen, PA 19428-2959,

Chemical Engineers' Handbook. 1950. John H. Perry, Editor. McGraw-Hill Book Co., N.Y., p. 800-808

Cohen, Y., H. Taghavi and P. A. Ryan. 1988. Chemical Volatilization in Nearby Dry Soils under Non-Isothermal Conditions. J. Environ. Qual. vol 17, no. 2, pp. 198-204.

Dungan, R. S.; Stork, A.; Frankenberger, Jr., W.T. 2000. A Wind Tunnel for Measuring Selenium Volatilization under Field-Like Conditions. Jo. Environmental Quality, 29: 460-466

Fountain, K. F., Thibodeaux, L. J., Valsaraj, K. T., Ravikrishna, R. "PAH Volatilization From Dredged Material Under IHC/CDF-Like Conditions: Wind Tunnel Flux Measurements and Modeling." 2005. 179p.

Fuller, E. N., Schettler, P. D. and Giddings, J. C., *Ind. Eng. Chem*., **58**(5), 18 (1966).

Global Security. "Dredges." http://www.globalsecurity.org/military/systems/ship/dredges.htm (accessed March 2005)

Great Lakes Dredging Team (GLDT). "Confined Disposal Facilities Fact Sheet." http://www.glc.org/dredging/outreach/cdffs.html (accessed March 2005)

International Association of Dredging Companies (IADC). "Environmental Developments." http://www.iadc-dredging.com/equip1.html (accessed March 2005)

Jury, W. A., R. Grover, W. F. Spencer and W. J. Farmer. 1980. Modeling Vapor Losses of Soil-Incorporated Triallate, Soil Sci. Soc. Amer. J., vol 44 p. 445-450.

Jury, W. A., W. F. Spencer and W. J. Farmer. 1983(I), 1984a(II), 1984b(III), 1984c(IV). Behavior Assessment Model for Trace Organics in Soil. I. Model Description. J. Environ. Quality. vol 12, no 4, p.558. II. Chemical Classification and Parameter sensitivity. J. Environ. Quality., vol 13, no 4, pp. 567-572. III. Application of Screening Model. J. Environ. Quality. vol. 13, no.V, pp. 573-578. IV. Review of Experimental Evidence. J. Environ. Qual. vol. 13. no. 4, pp. 1984-1986.

Mayer, R. J. Letey and W. J. Farmer. 1974. Models For Predicting Volatilization of Soil-Incorporated Pesticides. Soil Sci. Soc. Amer. Proc. vol 38, pp. 563-568.

Naval Facilities Engineering Service Center (NFESC). "In-Situ Capping." http://enviro.nfesc.navy.mil/erb/restoration/technologies/remed/contain_remove/cr-04.asp (accessed March 2005)

Price, R. A.; Skogerboe, J. G. and Lee, C.R. 1996. A Rainfall Simulator/Lysimeter System for Predicting Surface-Runoff Water Quality. Water Quality '96; p. 439-441

Ravikrishna, R, et al. 2001. Air emission flux from contaminated dredged materials stored in a pilot-scale confined disposal facility. J. Air & Waste Management Association. 51:361-373

Rochne, K.J., M. Shor, L.Y. Young, G. L.Taghon and D. S. Kasson. 2002. Environmental Science & Technology, vol. 30, No. 12, p. 2636-2644.

Ruscheweyh, H. 1984. A Mixing System for Gas Flow. Jo. Wind Engineering and Industrial Aerodynamics, 16: 189-199

Saichek, R., 2003. The Collection of Water and Sediment Samples from Indiana Harbor and Canal, CELRC-TS-HE. USACE, Chicago District. USAERDC, WES, Vicksburg, MS.

Sediment Management Work Group (SMWG). "Technology and Alternative Development and Screening." http://www.smwg.org/products/decisiontree/feasibility/tabled-1.pdf (accessed March 2005)

Schroeder, P. R. 2000. "Leachate screening considerations," DOER Technical Notes Collection (ERDC TN-DOER-C16), U.S. Army Engineer Research and Development Center, Vicksburg, MS. *www.wes.army.mil/el/dots/doer*

Springer, C., K.T. Valsaraj and L.J. Thibodeaux, "Emissions of Volatile Organics Chemicals from Landfills and Waste Piles", Final Report to USEPA Municipal Environmental Research Laboratory Solid and Hazardous Waste Research Division. Cincinnati, Ohio. Dec. 1984

Thibodeaux, L. J., et al. 1985. "Air/Soil Exchange Coefficients," Chapter 4 in W. B. Neely and G. E. Blau, Eds., Environmental Exposure from Chemicals, Vol. 1, CRC Press, Boca Raton, Fl.

Thibodeaux, L. J. 1989. "Theoretical Models for Evaluation of Volatile Emissions to Air During Dredged Material Disposal with Applications to New Bedford Harbor, Massachusetts," Miscellaneous Paper EL-89-3, US Army Engineer Waterway Experiment Station, Vicksburg, MS.

Thibodeaux, L. J., Poulin, M., Even, S. (1994). "A model for enhanced aeration of streams by motor vessels with application to the Seine river." *J. of Haz. Mats.*, 37, 459-473.

Thibodeaux, L. J. 1996. "Chemodynamics- Environmental Movement of Chemicals in Air, Water, and Soil." John Wiley, New York (1979), 501 p. [ISBN 0-471-04720-1]

Thibodeaux, L. J., et al. 2002. Volatilization rates from dredged material and soils-A literature review. Final Report. USACE, Chicago District. USAERDC, WES, Vicksburg, MS.

Thibodeaux, L. J., 2003. Calibration of the IHC CDF Emission Model. Memorandum to Le T. Thai, USACE Chicago District. October 28, 2002. 7p.

USEPA Pilot-Scale Demonstration of Sediment Washing for the Treatment of Saginaw River Sediments. EPA 905-R94-09. July 1994.

Valsaraj, K.T., R. Ravikrishna, B. Choy, D.D. Reible, L. J. Thibodeaux, C. B. Price, S. Yost, J. M. Brannon and T. E. Myers. 1999. Environmental Science & Technology. 33, 142-144

APPENDIX A

INPUT TO DOU MODEL SAMPLE CALCULATIONS (P 39)

Chemical Properties

$w_A := 3380 \frac{mg}{kg}$ "Sediment loading concentration in DOU (mg/kg)"

$\rho_{Astar} := 0 \frac{kg}{L}$ "Chemical concentration in air above DOU (mg/L)"

$K_{A32} := 260 \frac{L}{kg}$ "Sediment/Water partition coefficient for chemical A (L/kg)"

$D_{A2} := 7.5 \cdot 10^{-6} \frac{cm^2}{s}$ "Diffusivity of chemical A in water (cm^2/s)"

$H_x := 0.01980$ "Henry's constant for chemical A (unitless)"

Mass Transfer Coefficients

$k_{A1} := 3.476 \times 10^3 \frac{cm}{hr}$ "Air-side at air/water interface MTC of chemical A (cm/hr)"

$k_{dredge} := 3 \frac{cm}{hr}$ "Liquid-side at air/water interface MTC of chemical A from dredge (cm/hr)"

$k_{flow} := 0.046 \frac{cm}{hr}$ "Liquid-side at air/water interface MTC of chemical A from water flow (cm/hr)"

$k_{wind} := 1.611 \cdot \frac{cm}{hr}$ "Liquid-side at air/water interface MTC of chemical A from wind flow (cm/hr)"

$'K'_{A2} := 1.618 \frac{cm}{hr}$ "Overall natural surface liquid-side at air water interface MTC of chemical A (cm/hr)"

$'K_{A2} := 4.362 \frac{cm}{hr}$ "Overall forced surface liquid-side at air water interface MTC of chemical A (cm/hr)"

DOU Specification

$\rho_{32NC} := 50\frac{gm}{L}$ "TSS in natural zone of DOU (gm/L)"

$\rho_{32FC} := 500\frac{gm}{L}$ "TSS in forced zone of DOU (gm/L)"

$Q_w := 0.5\frac{m^3}{s}$ "Total river water volumetric flowrate (m^3/s)"

$v_{wind} := 9.261mph$ "Wind velocity (mph-no units for input)"

$w := 100m$ "Width of DOU (m)"

$h := 15m$ "Height of water column in DOU (m)"

$v_{water} := 7.456 \times 10^{-4} \cdot mph$ "Velocity of water into DOU (m/s)"

$A_{DOU} := 1569m^2$ "Area of DOU (m^2)"

$\tau_{DOU} := 13.075hr$ "Residence time for flow in DOU (hr)"

$P_D := 300hp$ "Power of dredge (hp)"

$A_{FDOU} := 473.8m^2$ "Area of forced convective zone in DOU (m^2)"

$A_{NDOU} := 1095.2m^2$ "Area of natural convective zone in DOU (m^2)"

$\tau_{FDOU} := 3.948hr$ "Residence time for flow in foced zone of DOU (hr)"

$\tau_{NDOU} := 9.127hr$ "Residence time for flow in natural zone of DOU (hr)"

APPENDIX B

INPUT TO PCDF MODEL SAMPLE CALCULATIONS (P 85)

Chemical Properties

$K'_{a32} := 260 \frac{L}{kg}$ "Chemical partition coefficient from sediment to water (L/kg)"

$H_\rho := 0.0198$ "Henry's constant for chemical (dimensionless)"

$w_a := 2.65 \cdot \frac{mg}{kg}$ "Dredge area sediment loading concentration (mg/kg)"

Mass Transfer Coefficient

$'k_{a21ee} := 1.878 \frac{cm}{hr}$ "Liquid-side local mass transfer coefficient for ethyl ether (cm/hr)"

$'k_{a21} := 1.395 \frac{cm}{hr}$ "Liquid-side local mass transfer coefficient for chemical A (cm/hr)"

$"k_{a12wv} := 2996.5 \frac{cm}{hr}$ "Gas-side local mass transfer coefficient for water vapor (cm/hr)"

$"k_{a12} := 1.341 \times 10^3 \frac{cm}{hr}$ "Gas-side local mass transfer coefficient for chemical A (cm/hr)"

$'K_{a2} := 1.325 \frac{cm}{hr}$ "Mass transfer coefficient from water to air (cm/hr)"

$"K_{a3} := 3.095 \frac{cm}{hr}$ "Mass transfer coefficient from sediment to water (cm/hr)"

DOU Specification

$\rho_3 := 2.41\frac{gm}{cm^3}$ "Particle density of dredged material (gm/ml)"

$\rho_b := 1.1\frac{gm}{cm^3}$ "Bulk density of dredged material (gm/ml)"

$Q_{ds} := 250\frac{yd^3}{hr}$ "Dredge rate (yd^3/hr)"

$\varepsilon_2 := 0.7$ "DOU water porosity of dredged sediment (dimensionless)"

$\varepsilon_I := 0.7$ "Initial CDF water porosity of dredged sediment (dimensionless)"

$\varepsilon_F := 0.3$ "Final CDF water porosity of dredged sediment (dimensionless)"

$A_{stot} := 35.\,lacre$ "CDF total surface area (acre)"

$A_s := 1acre, 2acre .. A_{stot}$ "CDF surface area interval and range for final mass evaporation rate (acre)"

$v_1 := 10mph$ "Wind velocity in the x-direction (mph)"

$Q_P := 1.312\frac{ft^3}{s}$ "Dredge site pore water volumetric flowrate (ft^3/s)"

$m_P := 38421.1\frac{gm}{s}$ "Dredge site solid mass flowrate (gm/s)"

$\rho_{32o} := 170\frac{gm}{L}$ "Suspended solids concentration in influent (gm/L)"

$Q_I := 7.981\frac{ft^3}{s}$ "CDF water volumetric flowrate (ft^3/s)"

$Q_S := 2.878\frac{ft^3}{s}$ "Water volumetric flowrate to CDF sediment (ft^3/s)"

$Q_X := 1.151\frac{ft^3}{s}$ "Water volumetric flowrate to water column from consolidation (ft^3/s)"

$Q_B := 1.727\frac{ft^3}{s}$ "Water volumetric flowrate to water column from consolidation (ft^3/s)"

$Q_R := 6.254\frac{ft^3}{s}$ "Recycle water volumetric flowrate (gm/s)"

$Q_M := 0.415\frac{ft^3}{s}$ "Makeup water volumetric flowrate (ft^3/s)"

$m_M := 0\frac{gm}{s}$ "Makeup water solid mass flowrate (gm/s)"

$m_D := 38.421\frac{kg}{s}$ "Total dredge solids flowrate (gm/s)"

$v_x := 0.083 \frac{cm}{hr}$ "Water velocity in the x-direction (m/s)"

$v_s := 0.207 \frac{cm}{hr}$ "Water velocity in the x-direction (m/s)"

$\rho''_{a2} := 0 \frac{mg}{L}$ "Chemical concentration in air above CDF (mg/L)"

$\rho_{a2P} := 10.192 \frac{ngm}{cm^3}$ "Chemical concentration in sediment pore water at dredge site (ngm/cm^3)"

$\rho_{32} := 8.764 \times 10^3 \cdot \frac{ngm}{cm^3}$ "Suspended solids concentration in basin (mg/L)"

VITA

Kenneth Alexander Fountain was born on June 21, 1978, in Gulfport, Mississippi, to Kenneth A. and Barbara J. Fountain. Kenneth attended high school at St. Martin High in Ocean Springs, Mississippi. After graduation, he decided to pursue a career in chemical engineering due to his interest in both math and chemistry. He graduated *magna cum laude* from Mississippi State University in December of 2000 with a Bachelor of Science in Chemical Engineering. With nearly three years of work experience, Kenneth decided to attend graduate school at Louisiana State University to attain a Master of Science in Chemical Engineering degree. This thesis concludes the degree program requisites upon graduation.